



# 1 Influence of anthropogenic emissions on the composition of highly 2 oxygenated organic molecules in Helsinki: a street canyon and urban 3 background station comparison

4 Magdalena Okuljar<sup>1</sup>, Olga Garmash<sup>2\*</sup>, Miska Olin<sup>2</sup>, Joni Kalliokoski<sup>2</sup>, Hilikka Timonen<sup>3</sup>, Jarkko V.  
5 Niemi<sup>4</sup>, Pauli Paasonen<sup>1</sup>, Jenni Kontkanen<sup>1\*\*</sup>, Yanjun Zhang<sup>1\*\*\*</sup>, Heidi Hellén<sup>3</sup>, Heino Kuuluvainen<sup>2</sup>,  
6 Mina Aurela<sup>3</sup>, Hanna E. Manninen<sup>4</sup>, Mikko Sipilä<sup>1</sup>, Topi Rönkkö<sup>2</sup>, Tuukka Petäjä<sup>1</sup>, Markku  
7 Kulmala<sup>1</sup>, Miikka Dal Maso<sup>2</sup> and Mikael Ehn<sup>1</sup>

8 <sup>1</sup>Institute of Atmospheric and Earth System Science, Faculty of Science / Physics, Faculty of Science, University of  
9 Helsinki, FI-00014, Helsinki, Finland

10 <sup>2</sup>Aerosol Physics Laboratory, Physics Unit, Tampere University, PO Box 692, FI-33014, Tampere, Finland

11 <sup>3</sup>Atmospheric Composition Research, Finnish Meteorological Institute, Helsinki, Finland

12 <sup>4</sup>Helsinki Region Environmental Services Authority, HSY, PO Box 100, FI-00066, Helsinki, Finland

13 \*Now at the Department of Atmospheric Sciences, University of Washington, Seattle, WA, United States

14 \*\*Now at CSC – IT Center for Science Ltd., Espoo, Finland

15 \*\*\*Now at Univ. Lyon, Université Claude Bernard Lyon 1, CNRS, IRCELYON, 69626 Villeurbanne, France

16 *Correspondence to:* Magdalena Okuljar (magdalena.okuljar@helsinki.fi)

17 **Abstract.** Condensable vapors, including highly oxygenated organic molecules (HOM), govern secondary organic  
18 aerosol formation and thereby impact the amount, composition, and properties (e.g. toxicity) of aerosol particles. These  
19 vapors are mainly formed in the atmosphere through the oxidation of volatile organic compounds (VOCs). Urban  
20 environments contain a variety of VOCs from both anthropogenic and biogenic sources, as well as other species, for  
21 instance nitrogen oxides (NO<sub>x</sub>), that can greatly influence the formation pathways of condensable vapors like HOM.  
22 During the last decade, our understanding of HOM composition and formation has increased dramatically, with most  
23 experiments performed in forests or in heavily polluted urban areas. However, studies on the main sources for condensable  
24 vapors and secondary organic aerosols (SOA) in biogenically influenced urban areas, such as suburbs or small cities, has  
25 been limited. Here, we studied the HOM composition, measured with two nitrate-based chemical ionization mass  
26 spectrometers and analyzed using positive matrix factorization (PMF), during late spring at two locations in Helsinki,  
27 Finland. Comparing the measured concentrations at a street canyon site and a nearby urban background station, we found  
28 a strong influence of NO<sub>x</sub> on the HOM formation at both stations, in agreement with previous studies conducted in urban  
29 areas. Even though both stations are dominated by anthropogenic VOCs, most of the identified condensable vapors  
30 originated from biogenic precursors. This implies that in Helsinki anthropogenic activities mainly influence HOM  
31 formation by the effect of NO<sub>x</sub> on the biogenic VOC oxidation. At the urban background station, we found condensable  
32 vapors formed from two biogenic VOC groups (monoterpenes and sesquiterpenes), while at the street canyon, the only  
33 identified biogenic HOM precursor was monoterpenes. At the street canyon, we also observed oxidation products of  
34 aliphatic VOCs, which were not observed at the urban background station. The only factors that clearly correlate  
35 (temporally and composition-wise) between the two stations contained monoterpene-derived dimers. This suggests that  
36 HOM composition and formation mechanisms are strongly dependent on localized emissions and the oxidative  
37 environment in these biogenically influenced urban areas, and they can change considerably also within distances of one  
38 kilometer within the urban environment.

39 1. Introduction



40 Urban environments can contain various anthropogenic and biogenic sources of volatile organic compounds (VOCs).  
41 Biogenic emissions come mostly from urban vegetation, for example, trees and bushes in parks, gardens, and may contain  
42 biogenic volatile organic compounds (BVOCs) such as isoprene, monoterpenes (MT), or sesquiterpenes. The sources of  
43 anthropogenic emissions consist of traffic, industrial processes and production of consumer goods, and volatile chemical  
44 products (VCP) (Li et al., 2022; Koppmann, 2007; Watson et al., 2001). Gas-phase compounds emitted from  
45 anthropogenic sources contain trace gases, including nitrogen oxides ( $\text{NO}_x$ ), as well as anthropogenic volatile organic  
46 compounds (AVOCs), for example aromatic compounds or aliphatic hydrocarbons (Timonen et al., 2017; McDonald et  
47 al., 2018). In densely populated areas, VCPs can dominate AVOCs concentrations and compounds typically known as  
48 BVOC (e.g., monoterpenes) are also emitted from anthropogenic sources, such as personal care products and cleaning  
49 agents (Gkatzelis et al., 2021; Li et al., 2022).

50 Under atmospheric conditions, VOCs can undergo oxidation to form condensable vapors (Pandis et al., 1992; Ehn et al.,  
51 2014). The most common ambient oxidants are ozone ( $\text{O}_3$ ), hydroxyl radical (OH), and nitrate radical ( $\text{NO}_3$ ) (Wayne,  
52 2000).  $\text{O}_3$  is a trace gas produced in the troposphere mostly by photolysis of  $\text{NO}_2$  (Liu et al., 1980), and present in the  
53 ambient air during the entire day.  $\text{O}_3$  can oxidize only VOC containing at least one double or triple bond, or, with a  
54 slower reaction rate, carbonyls (Bianchi et al., 2019). OH is a short-lived, highly-reactive compound produced mostly by  
55 the photolysis of  $\text{O}_3$  (Crutzen et al., 1999), thus OH is present in the atmosphere mainly during the daytime.  $\text{NO}_3$  is a  
56 product of the reaction between  $\text{O}_3$  and  $\text{NO}_2$ , which gets rapidly destroyed by photolysis and reactions with NO during  
57 the daytime (Wayne et al., 1991). Both radicals can react with most closed-shell VOCs (Seinfeld and Pandis, 2016), but  
58 in the atmosphere,  $\text{NO}_3$  reacts mostly with alkenes while OH reacts with almost all compounds, including aromatic  
59 hydrocarbons (Seinfeld and Pandis, 2016). Oxidation of VOCs almost always leads to peroxy radical ( $\text{RO}_2$ ) intermediates,  
60 typically with long enough lifetimes to participate in bimolecular reactions, primarily with NO,  $\text{HO}_2$ , or other  $\text{RO}_2$ . The  
61  $\text{RO}_2$  may also undergo various unimolecular isomerizations, and both these and the bimolecular reactions can lead to  
62 either propagation or termination of the organic radical (Bianchi et al., 2019). The structure of the final product depends  
63 on multiple factors, including the structure of the initial VOC and the “oxidative conditions”, meaning available oxidants  
64 and the bimolecular reaction partners. The latter can be referred to as “terminators” when they terminate the oxidation  
65 process, and in some cases the product composition can tell a lot about the oxidative conditions. Additionally,  $\text{NO}_2$  can  
66 terminate oxidation chain in reaction leading in most cases, which decompose back to substrates (Atkinson and Arey,  
67 2003). For example,  $\text{RO}_2$  termination by NO and oxidation by  $\text{NO}_3$  can produce organic nitrogen compounds (ONCs),  
68 organonitrates (Atkinson and Arey, 2003; Bianchi et al., 2019), while  $\text{RO}_2$  termination by  $\text{NO}_2$  can form relatively  
69 unstable peroxy nitrates.  $\text{RO}_2$  cross reactions are the only reactions that can form accretion products, ROOR, referred to  
70 here as “dimers” (Valiev et al., 2019).

71  $\text{RO}_2$  intermediates can also undergo autoxidation, where the  $\text{RO}_2$  isomerizes through a hydrogen shift (H-shift) creating  
72 an alkyl radical to which molecular oxygen can attached (Bianchi et al., 2019; Ehn et al., 2014; Crouse et al., 2013). In  
73 the end, a new, more oxidized  $\text{RO}_2$  is formed, which can either undergo additional H-shifts or bimolecular reactions, with  
74 both potentially terminating or propagating the oxidation (Bianchi et al., 2019) chain. In cases where the radical can  
75 undergo multiple autoxidation H-shifts, the end product can reach high enough oxidation levels to be classified as HOM  
76 (Bianchi et al., 2019). The structure of a VOC strongly influences its propensity to undergo autoxidation and,  
77 consequently, the molar yield of HOM. This results in the very variable HOM yields, which can reach high values for  
78 different anthropogenic and biogenic compounds (Molteni et al., 2018; Bianchi et al., 2019; Garmash et al., 2020).



79 Differences in the structural composition affect both the physical and chemical properties of HOM, with more oxidized  
80 products typically being less volatile (Kroll and Seinfeld, 2008). However, the exact functionalities are important, and  
81 e.g. oxygen atoms in nitrate groups lower the volatility much less than if the oxygen was found in some other functional  
82 group (Kroll and Seinfeld, 2008). In general, the high oxygen content of HOM makes them an important contributor to  
83 secondary organic aerosol (SOA) formation, influencing e.g. air quality.

84 During the last decade, HOM formation from biogenic emissions have been extensively studied in forests (Ehn et al.,  
85 2014; Yan et al., 2016; Bianchi et al., 2017; Massoli et al., 2018), and in agricultural environments (Kürten et al., 2016).  
86 Recently, research showed that also the oxidation of AVOCs can noticeably contribute to the HOM population (Molteni  
87 et al., 2018; Garmash et al., 2020; Wang et al., 2021) and SOA formation (Timonen et al., 2017). Additionally, NO<sub>x</sub> can  
88 alter the HOM formation mechanism and influence SOA formation (Fry et al., 2014; Ng et al., 2017; Pullinen et al., 2020;  
89 Mutzel et al., 2021). Due to these findings, the research on condensable vapors and their origin focused stronger on urban  
90 environments, especially very polluted ones, heavily influenced by anthropogenic emissions (Brean et al., 2019; Liu et  
91 al., 2021; Guo et al., 2022b; Nie et al., 2022; Yan et al., 2022). In very polluted environments, formation of condensable  
92 vapors is greatly impacted by NO<sub>x</sub> (Brean et al., 2019; Liu et al., 2021; Guo et al., 2022b; Nie et al., 2022; Yan et al.,  
93 2022) and HOM composition is often dominated by AVOC precursors (Nie et al., 2022).

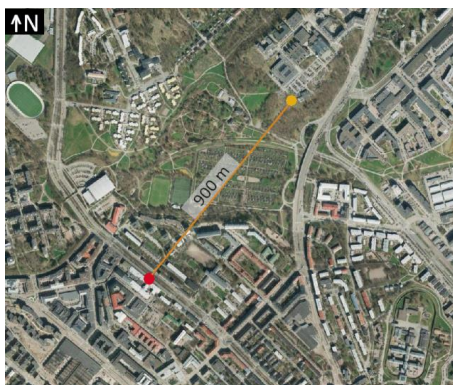
94 While the composition and formation of condensable vapors have been studied in the above-mentioned forests and highly  
95 polluted locations, environments with considerable influence from both anthropogenic and biogenic emission sources  
96 have received much less attention. Such areas include urban environments with lots of green areas, for example suburbs,  
97 or cities surrounded by large forests. A better understanding of such locations may also help to assess the impact on air  
98 quality from adding vegetation such as green roofs to already built-up areas. Helsinki is an example of a city with forests  
99 in close proximity, and Saarikoski et al. (2023) estimated that there, even at a street canyon site strongly affected by traffic  
100 emissions, BVOCs are the main contributor to oxidation products. While Saarikoski et al. (2023) measured only the  
101 composition of VOCs, and not their oxidation products, this finding makes us expect that the relative role of BVOCs is  
102 even higher for HOM, as BVOCs typically have higher propensity for autoxidation than AVOC (Bianchi et al., 2019).  
103 Another important aspect to consider is the spatial representativeness of typical urban measurements. As cities are very  
104 inhomogeneous in terms of local emissions and the oxidative environment, and HOM are short-lived compounds, HOM  
105 studies in urban environments that were performed at one specific location may not be comparable to other nearby  
106 locations with different urban sub-environments.

107 Here we investigate the composition of condensable vapors at two nearby stations in Helsinki, which are differently  
108 influenced by anthropogenic emissions. The first station is located in a busy street canyon while the second is in an urban  
109 background area, at less densely built part of Helsinki, 150 meters from the nearest busy road. We studied the composition  
110 of condensable vapors, mostly HOM, at these sites using two nitrate-based chemical ionization mass spectrometers. To  
111 identify different HOM types from the mass spectra and connect them to different formation pathways, we applied  
112 Positive Matrix Factorization (PMF) to separate co-varying species. We compared the drivers of HOM formation between  
113 the two urban sub-environments and explored the roles of biogenic and anthropogenic emissions on HOM composition,  
114 in order to understand how these can affect the air quality in urban environments with a strong biogenic influence.

115 2. Methods



116 We measured the composition of condensable vapors at two stations in Helsinki situated in contrasting environments: the  
117 Helsinki Region Environmental Services Authority (HSY) air quality station (60°11'47.0'' N, 24°57'07.7'' E) and the  
118 Station for Measuring Ecosystem-Atmosphere Relations (SMEAR III, 60°12'10.4'' N, 24°57'40.2'' E) (Fig. 1). The HSY  
119 supersite is located at a street canyon, less than a meter from Mäkelänkatu street (around 28 000 vehicles/weekday)  
120 (Kuuluvainen et al., 2018). SMEAR III is 900 m north-east of the HSY station and with 150 m distance from the closest  
121 busy road (Hämeentie street). SMEAR III, is classified as an urban background station (Järvi et al., 2009). The  
122 neighborhood of these stations was previously described in Okuljar et al. (2021). Here we refer to them as “street canyon”  
123 (later also “SC”) and “urban background station” (later also abbreviated “UB”), respectively.  
124 The measurement campaign was conducted during 11 May 2018 – 03 June 2018 at the urban background station and 27  
125 April 2018 – 24 May 2018 at the street canyon. The measurement period was during change of season and by 14 May  
126 2018 the deciduous trees in the surrounding area had fully developed their leaves. To study the influence of traffic  
127 emissions, we analyzed separately the data measured during workdays as well as only during weekends and public  
128 holidays (1 May 2018 and 10 May 2018). We refer to them as ‘workdays’ and ‘weekends’, respectively. As the nighttime  
129 concentrations are often influenced by the emission from the previous day, we separate these categories in 24 h periods  
130 starting at 4 a.m. The corresponding analysis of size distribution of 1-1000 nm particles measured during the same time  
131 at both stations in Helsinki is presented by Okuljar et. al. (2021).



132

133 Figure 1. Orthophotograph of stations in street canyon (red) and in an urban background environment (yellow) made on  
134 May 7<sup>th</sup>, 2018. The photograph was provided by The City of Helsinki map service (CC BY 4.0).

### 135 2.1. Condensable vapor measurements

136 The composition of condensable vapors was measured simultaneously at both stations by two nitrate-ion based chemical  
137 ionization atmospheric pressure interface (CI-API-TOF) mass spectrometers (MS) (Jokinen et al., 2012). Nitrate ions  
138 ( $\text{NO}_3^-$ ), produced by interactions between soft x-ray and sheath air containing nitric acid ( $\text{HNO}_3$ ), binds to the analyzed  
139 compound through hydrogen bonds or charges the analyte via proton transfer reactions.  $\text{NO}_3^-$  is primarily selective  
140 towards organic molecules containing at least two suitably positioned hydroxyl (-OH) or hydroperoxyl groups (-OOH)  
141 (Hytinen et al., 2015), or compounds with higher gas-phase acidity than  $\text{HNO}_3$ . After the sample gets ionized, the ions  
142 are focused in the API module and ultimately separated in the time-of-flight (TOF) analyzer based on their mass-to-charge  
143 ratio ( $m/Q$ , reported in units of Th). The CI-API-TOF and its working principle was described in detail by Jokinen et al.



144 (2012). The resolving power of the MS at both stations was approximately 3000–4000 Th/Th for signals with m/Q higher  
145 than 200 Th. The mass spectra were analyzed using the software package tofTools (Junninen et al., 2010).

146 In measured mass spectra, we observed multiple peaks at every m/Q. To perform high-resolution (HR) analysis requires  
147 us to fit closely set signals and could increase uncertainties of results. Therefore, most of our analysis is based on unit  
148 mass resolution (UMR) data and HR analysis follow only when we can narrow it usage. Additionally, we noted that  
149 condensable vapor measurement at street canyon had lower transmission for higher m/Q than at urban background station.

150 Here, we discuss quantitative changes in condensable vapors based on their measured signal in counts per second (cps)  
151 normalized by the cps of the reagent ions, using the unit ncps (normalized cps). The ambient concentrations can be  
152 estimated by using previously determined instrument-specific calibration coefficients for sulfuric acid (Okuljar et al.,  
153 2021) equal to  $4 \cdot 10^9 \text{ cm}^{-3}$  for the street canyon station and  $7 \cdot 10^9 \text{ cm}^{-3}$  for the urban background station. However, usage  
154 of these calibration coefficient determined for sulfuric acid to calculate HOM concentration comes with very large  
155 uncertainties, and we therefore concentrate on comparison of ion signal strength.

## 156 2.2. VOC measurements

157 VOC concentrations were measured at the street canyon with an offline method in which ambient samples were first  
158 collected on a Tenax TA-Carbopack B sorbent tube and later analyzed by thermal desorption gas chromatography coupled  
159 with mass spectrometry (TD-GC-MS). We measured VOC concentrations during the period 15 – 25 May 2018 with 4 h  
160 time resolution. 13 analytes were classified as AVOCs: benzene, toluene, ethylbenzene, p/m-xylene, styrene, o-xylene,  
161 propylbenzene, 3-ethyltoluene, 4-ethyltoluene, 1,3,5-trimethylbenzene, 2-ethyltoluene, 1,2,4-trimethylbenzene, and  
162 1,2,3-trimethylbenzene, and 15 as BVOCs: monoterpenoids ( $\alpha$ -pinene, camphene,  $\beta$ -pinene,  $\Delta^3$ -carene, p-cymene, 1,8-  
163 cineol, limonene, terpinolene), terpene alcohol (linalool), an oxidation product of  $\beta$ -pinene (nopinone), bornyl acetate,  
164 and sesquiterpenes (longicyclene, iso-longifolene,  $\beta$ -caryophyllene and  $\alpha$ - farnesene). More detailed description of the  
165 method can be found e.g. in Helin et al. (2020).

## 166 2.3. Other instrumentation

167 CO<sub>2</sub>, NO, NO<sub>2</sub>, SO<sub>2</sub> as well as meteorological variables were measured at both stations. Table S1 contains information  
168 about measurements of additional variables used in this paper.

## 169 2.4. Positive Matrix Factorization

170 Collected datasets from the measurement of condensable vapors at both stations consist of an enormous amount of  
171 information and it is challenging to filter data that contain relevant information for analysis of HOM formation. As both  
172 stations are located in a city, the composition of condensable vapors is dependent on different types of VOC sources as  
173 well as chemical and meteorological conditions. To extract relevant information, separate different pathways of HOM  
174 formation, and find processes affecting condensable vapor composition at both stations, we applied Positive Matrix  
175 Factorization (PMF) (Paatero, 1997; Paatero and Tapper, 1994; Paatero and Hopke, 2003). PMF is a multivariate factor  
176 analysis model which has been widely used on aerosol mass spectrometry data (Ng et al., 2011; Zhang et al., 2011; Chen  
177 et al., 2022) and more recently on ambient gas-phase chemical ionization mass spectrometry data (Yan et al., 2016;  
178 Massoli et al., 2018; Zhang et al., 2019; Liu et al., 2021; Nie et al., 2022).



179 We performed PMF analysis on three different  $m/Q$  ranges from UMR data at both stations: 200-350 Th, 350-500 Th,  
180 and 500-650 Th. In this paper, we will refer to these ranges as ranges 1, 2, and 3, respectively. The loss rate of HOM due  
181 to condensation is roughly a function of their mass (Peräkylä et al., 2020), thus, analyzing mass spectra in ranges allows  
182 us to group HOM with similar loss rates and focus specifically on separating the HOM sources (Zhang et al., 2020).  
183 Additionally, when a  $m/Q$  range has lower signal than other ranges, it will only have a minor weight on the PMF solution  
184 and relevant information may be lost (Zhang et al., 2020). Using  $m/Q$  ranges for PMF analysis is important especially at  
185 the street canyon as it may partly counteract the loss of information due to lower transmission for higher  $m/Q$ . The focus  
186 of our analysis is on compounds in a range of 200 to 650 Th as in this reach we can find majority of the condensable  
187 vapors containing  $C_{5-20}$ . Smaller  $m/Q$  are unlikely to condense, while larger  $m/Q$  had very low, or even negligible, signals.  
188 We prepared data and error matrices with 30 min time resolution, separately for each range at each station according to  
189 the methods described by Yan et al. (2016). To conduct PMF analysis we used the Igor-based interface Source Finder  
190 (SoFi, version 6.D) (Canonaco et al., 2013) and ME-2 solver (Paatero, 1999). Detailed information about data preparation  
191 and validation of PMF solutions can be found in S1.

192 To describe the chemical composition of ions in obtained factors, we determined the times for each factor when that factor  
193 had the highest relative contribution to the total signal and then fit peaks to the HR data to identify the key compounds.  
194 Choosing times when the analyte is dominant across all factors in the same  $m/Q$  range and at the same site is necessary  
195 to ensure that identified compound is correctly assigned to the factor. In this paper, we performed a more detailed  
196 interpretation only of chosen factors from each station, which we refer to further on as “selected factors”. A factor was  
197 chosen for further interpretation only when we could reasonably identify ions in it, and relate it to a real atmospheric  
198 source, i.e. not impurities. We refer to other factors as “not selected factors”. Examples of each type will be given later to  
199 better clarify this selection process.

## 200 2.5. Limitation of data for interpretation

201 There are several limitations for interpreting the data. At the street canyon, a low signal is observed for higher  $m/Q$ . That  
202 leads to a low signal-to-noise ratio (S/N) for HOM measured in range 2 and 3, and in some cases makes it impossible to  
203 identify the compounds. As a result of fast decrease of measured signal with an increase of  $m/Q$ , at the street canyon, over  
204 90 % of the signal of 200-650 Th is located in range 1. This could be caused by the low transmission for higher  $m/Q$  of  
205 the CI-API-TOF measurement at that station. Transmission is a result of voltage settings in CI-API-TOF, which are  
206 optimized for each instrument separately. Zha et al. (2018) showed that the ratio of the signal for the same sampled air  
207 measured by two CI-API-TOF can change drastically with an increase of  $m/Q$  due to the difference in the transmission  
208 between instruments. Thus, the highest uncertainty caused by inconsistent transmission between two instruments is  
209 observed in range 3. Nevertheless, this uncertainty does not influence identification of peaks that have sufficient S/N.

210 Due to the chemical complexity of the samples, we cannot achieve high accuracy of mass calibration on some of the  
211 measured days. This is the reason why we have performed PMF analysis on UMR data. Limitations of peak identification  
212 due to the MS resolution and the presence of multiple overlapping peaks also hinder the identification of some ions, and  
213 hence we are confident to report only the dominant ions in each factor. We are not able to report key compounds for  
214 factors that have minor contribution to their  $m/Q$  range or have too many similar peaks with other factors, as we cannot  
215 unambiguously assign identified compounds to these specific factors.





216 Lastly, we need to keep in mind that chemical ionization with  $\text{NO}_3^-$  is very selective, mostly towards highly functionalized  
 217 compounds. Overall, this ionization method is optimal for detection of HOM, however, it limits observations of other  
 218 oxidation products.

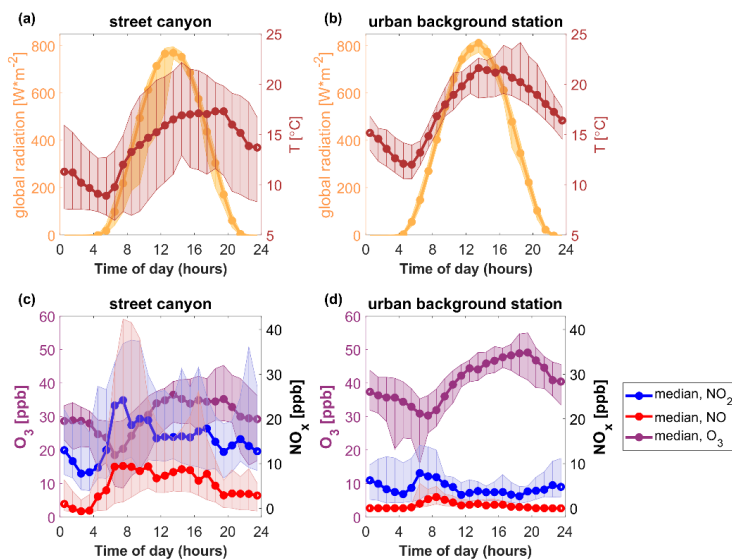
219 3. Results and discussion

220 We start this section by providing a short overview of the meteorological conditions during the campaign. In section 3.2,  
 221 we present our main findings, starting from the PMF results and the subsequent interpretations of important formation  
 222 pathways of condensable vapors at the two measurement sites. In the last part of this section, we discuss the potential  
 223 implications of our findings on the air quality in Helsinki.

224 Concerning notations, we focus our study on HOM, but we also detect abundant organic compounds which contain less  
 225 than six oxygen atoms, which do not classify as HOM. Thus, we often use a broader term ‘condensable vapors’ when  
 226 discussing observed products more broadly. In addition, we observe monomeric (mostly  $\text{C}_9\text{-C}_{10}$ ) and dimeric (mostly  $\text{C}_{19}\text{-}$   
 227  $\text{C}_{20}$ ) oxidation products of MT, which we refer to as ‘MT-derived monomers’ and ‘MT-derived dimers’, respectively. For  
 228 simplicity, we call factors containing monomeric oxidation products of MT ‘MT monomers’ while ‘MT dimers’ factors  
 229 contain of dimeric oxidation products of MT.

230 3.1. Overview of meteorological and trace gas conditions in Helsinki

231 Atmospheric conditions, for example local emissions and oxidative environment, influence HOM formation pathways.  
 232 To understand HOM formation mechanisms and their differences between studied sites, we first investigated  
 233 meteorological and chemical conditions at both stations. Figure 2 presents diurnal variations of measured variables that  
 234 can influence HOM formation pathways: global radiation, ambient temperature (T), and concentrations of  $\text{O}_3$ , NO, and  
 235  $\text{NO}_2$ . As mentioned earlier, the measurement periods overlapped but were not identical between the two stations.  
 236 Therefore, differences in campaign averages between sites are partly driven by differences in location and partly by  
 237 differences in time.



238



239 Figure 2. Diurnal variations of (a,b) global radiation and ambient temperature, and (c,d) NO, NO<sub>2</sub>, and O<sub>3</sub> concentrations  
240 at the street canyon (left) and urban background station (right). Presented data contain both workdays and weekends. The  
241 median diurnal variations are shown as solid lines with markers; 25<sup>th</sup> to 75<sup>th</sup> percentile ranges are presented as shaded  
242 areas. Time is local.

243 Diurnal variation of global radiation is similar between the two stations (Figure 2a,b), though with slightly more cloudy  
244 periods at the street canyon. Global radiation initiates photolysis reactions and, as a result, enhances the formation of OH  
245 and O<sub>3</sub> as well as the decomposition of NO<sub>3</sub>. Median temperatures varied between 12.0°C and 21.6°C at the urban  
246 background site and between 8.9°C and 17.3°C in the street canyon. Higher temperature at the urban background station  
247 can be explained by the difference in measurement periods as the measurements started two weeks later than in street  
248 canyon. During the period when measurements overlapped, the median temperature is very similar between stations  
249 reaching almost 22°C during daytime and dropping to 12-13.4°C during nighttime (figure not shown). The increase in  
250 temperature typically accelerates molecular reaction rates as well as enhances BVOCs emissions and evaporation rates.  
251 It can also affect HOM yields (Quelever et al., 2019).

252 At the urban background station, NO has a maximum between 8:00 and 9:00 (2.5 ppb) and it is negligible during  
253 nighttime. In contrast, at the street canyon, the median NO concentration was below the detection limit between 1:00 and  
254 3:00, after which it rapidly increased, levelling off at 7:00 and staying elevated (ca. 9 ppb) throughout the day until 17:00.  
255 That means NO can affect oxidation reactions more at the street canyon site, even during much of the night, when it stays  
256 at 4 ppb until early morning. In the context of VOC oxidation, the presence of NO likely causes the termination of the  
257 oxidation. In the absence of NO, termination reactions with RO<sub>2</sub> become more favorable. NO<sub>2</sub> and NO (Figure 2c,d)  
258 concentrations are up to 5 and 23 times higher at the street canyon than at the urban background station, respectively. At  
259 urban background site, O<sub>3</sub> reaches minimum median concentration at 7:00 (30.3 ppb) and maximum at 19:00 (49.1 ppb).  
260 At the street canyon, the corresponding values are 18.5ppb at 6:00 and 36.5 ppb at 13:00. During overlapping times  
261 between the sites, median O<sub>3</sub> concentration stays 5-25 ppb lower at street canyon than at urban background station (figure  
262 not shown). It could be partly associated with higher NO concentration in street canyon as NO reacts with O<sub>3</sub>. O<sub>3</sub> remains  
263 relevant for VOCs oxidation throughout the day. O<sub>3</sub> and NO<sub>2</sub> concentrations affect production of NO<sub>3</sub> and thus its  
264 concentration.

### 265 3.2. Characterization of PMF factors

266 In this subsection, we examine the HOM composition and formation at both stations by investigating PMF factors in all  
267 three m/Q ranges (200-350 Th, 350-500 Th, 500-650 Th); we focus our analysis on selected factors, their time-series, and  
268 diurnal variations (Fig. 3-4) as well as mass spectra (Fig. S2-3). We refer to PMF factors as SCX-Y or UBX-Y where SC  
269 is the street canyon, UB is the urban background station, X is the analyzed m/Q range (either 1, 2, or 3), and Y is the  
270 identifying number of the factor in that range. The factors also appear together with a descriptive name. As an example,  
271 “UB3-2: *MT dimers*” refers to the second PMF factor identified in mass range 3 at the urban background site and was  
272 found to mainly contain ions related to monoterpene-derived dimers. To understand the chemical composition of factors,  
273 we identify their key compounds with HR data (Table S2) as described in Sect. 2.5. All key compounds are detected as  
274 clusters with NO<sub>3</sub><sup>-</sup> or HNO<sub>3</sub>NO<sub>3</sub><sup>-</sup> and this is how we report them in Table S2 and on the mass spectra (Fig. S2-3 and S6-  
275 7); however, for clarity of the interpretation in this subsection, we write their chemical structures without the nitrate  
276 adducts.



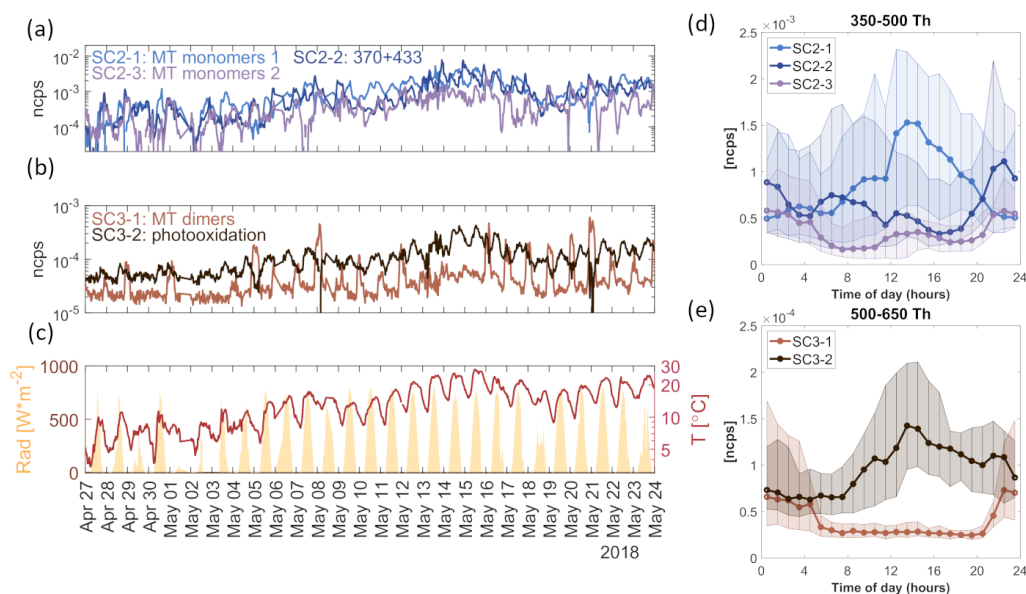


277

278 The PMF analysis involves several lengthy steps, including determining an optimal number of factors in the solution, as  
 279 well as interpreting sources for each factor based on the supporting data available. In this study, we had six data sets to  
 280 analyze (two sites and three mass ranges). As a result, we summarize the key characteristics of each factor and give an  
 281 interpretation in the main text and present more detailed description of the PMF analysis in the supplementary information  
 282 (SI) (Sect. S2 motivates the choice of factor numbers, Sect. S3 describes the main features of each factor, which lead to  
 283 the interpretations given in the main text). In the following sections, we first briefly describe the overall characteristics of  
 284 factors observed at the street canyon (Sect. 3.2.1) and at the urban background station (Sect. 3.2.2) after which we compare  
 285 HOM formation and composition between these sites (Sect. 3.2.3).

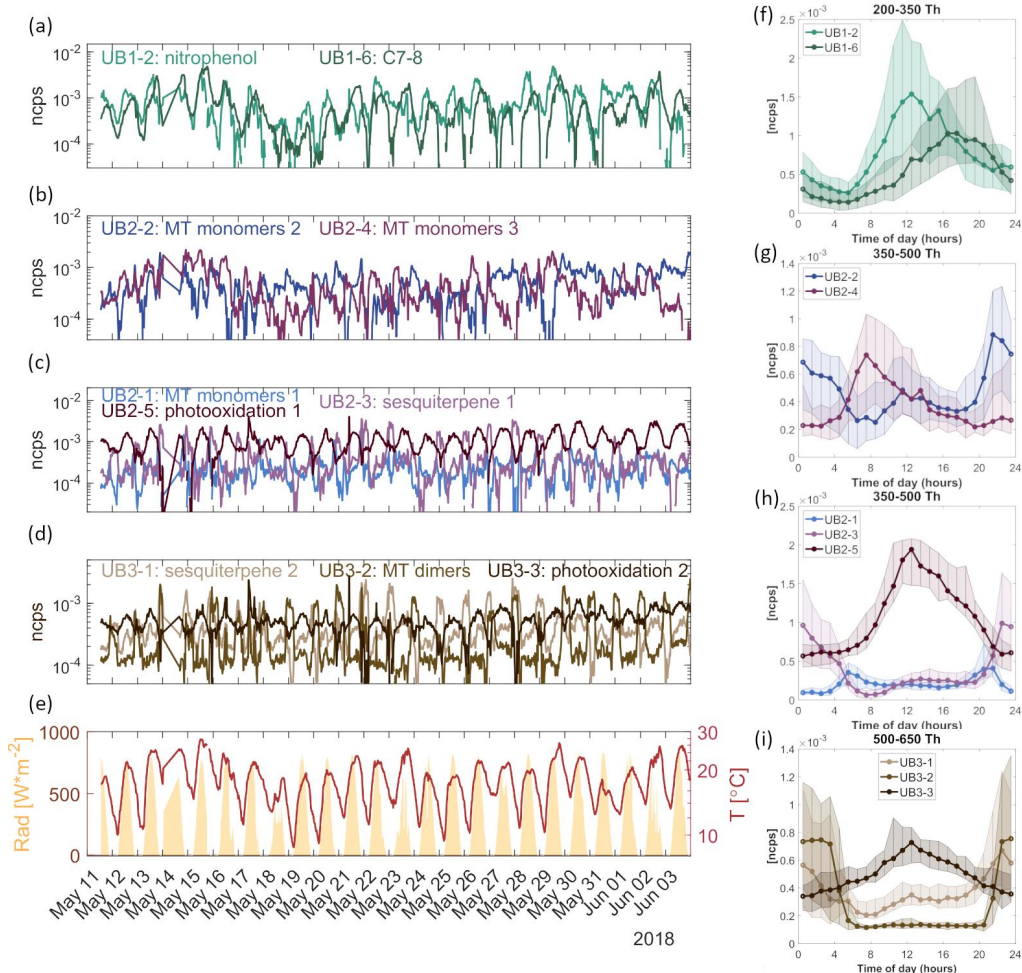
286

287 Only “selected” factors are described here, while characteristics of “not selected” factors are presented and described in  
 288 the SI (Sect. S3, Fig. S6-7, Table S3). Several reasons motivated us not to select factors for detailed discussion in the  
 289 main text. For example, a factor was not selected if it was a contamination or an artefact (e.g., containing mainly water  
 290 clusters isotopes) or if we were not confident in the meaningful separation of this factor by PMF method (this was the  
 291 case for the entire range 1 at the street canyon, as described below). Overall, we selected 5 out of 13 factors from the  
 292 street canyon and 10 out of 14 factors from the urban background station. These selected factors explain 34%, 100%, and  
 293 100% of the observed signal in ranges 1-3 at the urban background station and 0%, 64%, and 61% of the observed signal  
 294 in ranges 1-3 at the street canyon, respectively (Table 1, Fig. S3-4).



295

296 Figure 3. Time series of selected PMF factors (a-b), global radiation and ambient temperature (c), and diurnal variation  
 297 of PMF factors fractions (d-e) at street canyon (SC). The median diurnal variation is shown as a solid line with markers;  
 298 25th to 75th percentile ranges are presented as shaded areas. Y-axis in ncps indicates the measured signal in normalized  
 299 counts per second.



300

301 Figure 4. Time series of selected PMF factors (a-d), global radiation and ambient temperature (e), and diurnal variation  
 302 of PMF factors (f-i) at urban background station (UB). The median diurnal variation is shown as a solid line with  
 303 markers; the 25<sup>th</sup> and 75<sup>th</sup> percentile ranges are presented as shaded areas. Y-axis in ncps indicates the measured signal  
 304 in normalized counts per second.

305

### 3.2.1. Street canyon

306 Here, we very briefly describe factors observed at the street canyon site in each m/Q range. The main examination of the  
 307 factors is given in Sect. 3.2.3 where we also discuss them in relation to factors observed at the urban background station.  
 308 As indicated already above, PMF solutions for range 1 at the street canyon were inconclusive, and therefore all factors  
 309 from this range are classified as ‘not selected’. The main reason is that all factors had very similar temporal trends, mainly  
 310 correlating with temperature. This may be a result of most observed molecules being semi-volatile, and increased  
 311 temperatures lead to increased evaporation of these molecules. In any case, as PMF relies on temporal variability to  
 312 separate factors, too much co-variance makes PMF less reliable. Nevertheless, we believe there was some useful



313 information also in this range and will briefly discuss *SCI-1: nitrophenol 1*, *SCI-2: MT monomers 3*, and *SCI-5:*  
314 *nitrophenol & aliphatic* in this section.

315 **Range 1, 200-350 Th (Factors selected: 0/5)**

316 In range 1, all factors are affected by changes in ambient temperature (Fig. S6 and S10). Factors in range 1 have a daytime  
317 peak and nearly all of them could have been oxidized by OH or O<sub>3</sub> (Fig. S6, Table S3). Most of these factors are likely  
318 formed from AVOCs and contain nitrophenol (C<sub>6</sub>H<sub>5</sub>O<sub>3</sub>N) as well as other N-containing aromatics, such as nitroresol.  
319 Nitrophenol can be directly emitted from combustion or formed from benzene and phenol oxidation. The presence of  
320 nitrophenol in many factors can be explained by an abundance of benzene at the street canyon as it is the third most  
321 abundant VOC measured at the street canyon site (Fig. S8).

322 **Range 2, 350-500 Th (Factors selected: 3/5)**

323 In range 2, all selected factors respond to the changes in the ambient temperature (Fig. 3 and S10), especially factor SC2-  
324 1, which contains monomeric oxidation products of MT (MT-derived monomers) with nitrate functionalities. Factors  
325 SC2-2 and SC2-3 are highest during the night, but they also have local maxima during the day, which suggests that  
326 competing processes influence the formation of these factors and thus their diurnal pattern. SC2-3 may be inhibited by  
327 NO, as it decreases when NO reaches its daily maximum (Figure 3d). SC2-3 consists of MT-derived monomers, while  
328 SC2-2 is dominated by one single compound: C<sub>10</sub>H<sub>16</sub>O<sub>9</sub>N<sub>2</sub>.

329 **Range 3, 500-650 Th (Factors selected: 2/3)**

330 Range 3 contains one daytime and one nighttime factor. SC3-1 is a MT-derived dimer factor produced via oxidation by  
331 NO<sub>3</sub> and present during the night, when NO concentrations are low enough to allow RO<sub>2</sub> termination via RO<sub>2</sub> cross  
332 reactions. SC3-2 is a daytime factor containing HOM oxidized by OH. SC3-2 also has some signal from instrumental  
333 impurities containing fluorine (F-impurities), and undefined noise peaks.

334 3.2.2. Urban background station

335 Similar to the previous subsection, we describe briefly factors observed in all ranges at the urban background station.  
336 The discussion about these factors follows in Sect. 3.2.3, in which we compare factors found at both sites in Helsinki.

337 **Range 1, 200-350 Th (Factors selected: 2/6)**

338 Selected factors in range 1 contain daytime factors, from which UB1-6 is a factor correlating the best with the ambient  
339 temperature (Fig. 4 and S1). Time-series of UB1-6 correlates with O<sub>3</sub> (Fig 4a, Fig. S11) and it contains key compounds  
340 with C<sub>7-8</sub> atoms. These formulas have been detected earlier as products of MT oxidation in chamber studies (Yan et al.,  
341 2020) and in ambient measurement (Liu et al., 2021), however, they have also been identified as oxidation products of  
342 aromatic VOCs (Guo et al., 2022b). Since CI-API-TOF does not provide information about molecular structure, we cannot  
343 unambiguously determine the origin of this factor. In contrast to UB1-6, UB1-2 factor contains nitrophenol and likely  
344 originates from AVOCs. The diurnal variation of UB1-2 resembles the one expected for OH (Saarikoski et al., 2023).  
345 Both UB1-2 and UB1-6 contain ONCs and their oxidation was likely terminated by NO or NO<sub>2</sub>.

346 **Range 2, 350-500 Th (Factors selected: 5/5)**



347 Range 2 contains various daytime and nighttime factors (Fig. 4). Factor UB2-1 reaches the highest concentrations at 5  
348 am. and 10 pm., which corresponds to the time of sunrise and sunset during our measurement period. As this factor  
349 consists of MT-derived HOM with two N-atoms, we can speculate that they are formed from NO<sub>3</sub> oxidation of MT and  
350 terminated by NO. It is typically assumed that NO<sub>3</sub> and NO would not co-exist. However, simultaneous presence of NO<sub>3</sub>  
351 and NO when photolysis is just high enough to form NO but not to fully deplete NO<sub>3</sub> is a plausible explanation for the  
352 diurnal pattern of UB2-1.

353 UB2-2 and UB2-3 are both nighttime factors oxidized mainly by NO<sub>3</sub> and inhibited by NO during daytime. UB2-2  
354 contains MT-derived monomers and correlates with the MT-derived dimer factor (UB3-2). Following the diurnal cycle  
355 in Fig. 4g, it can be observed that when the concentration of UB2-2 decreases, the concentration of daytime MT-derived  
356 monomer factor, UB2-4, increases. Even though UB2-2 and UB2-4 both contain key compounds with C<sub>9-10</sub>, the molecular  
357 formulas are slightly different. Specifically, in UB2-2 key compounds contain one or three N-atoms while in UB2-4 they  
358 have zero or two N-atoms. UB2-2 and UB2-4 could thus be formed from competing HOM formation pathways from the  
359 same VOCs.

360 In contrast to other factors, UB2-3 consists of HOM with composition of C<sub>15</sub>H<sub>23</sub>O<sub>8,10-16</sub>N, based on which we conclude  
361 that this factor is formed from sesquiterpenes (C<sub>15</sub>H<sub>24</sub>, Richters et al., 2016). UB2-3 correlates very well with a  
362 corresponding sesquiterpene factor from range 3, UB3-1 (R=0.93) (Fig. S9). The last factor UB2-5 is a daytime factor  
363 which during noon corresponds to more than 50% of the measured signal (Fig. S5). It is most likely that UB2-5 is formed  
364 in OH oxidation.

### 365 **Range 3, 500-650 Th (Factors selected: 3/3)**

366 Range 3 at UB site contains two nighttime factors: sesquiterpene-derived UB3-1 factor, and MT-derived dimer UB3-2  
367 factor. Both factors consist of ONCs, products of NO<sub>3</sub> oxidation of BVOCs, and are inhibited by NO, being absent during  
368 the day as a result. UB3-3 is the only daytime factor (Fig. 4i) in range 3 and it consists of OH-oxidized HOM, F-impurities,  
369 and noise.

#### 370 3.2.3. Factor interpretation and comparison between urban background and street canyon sites

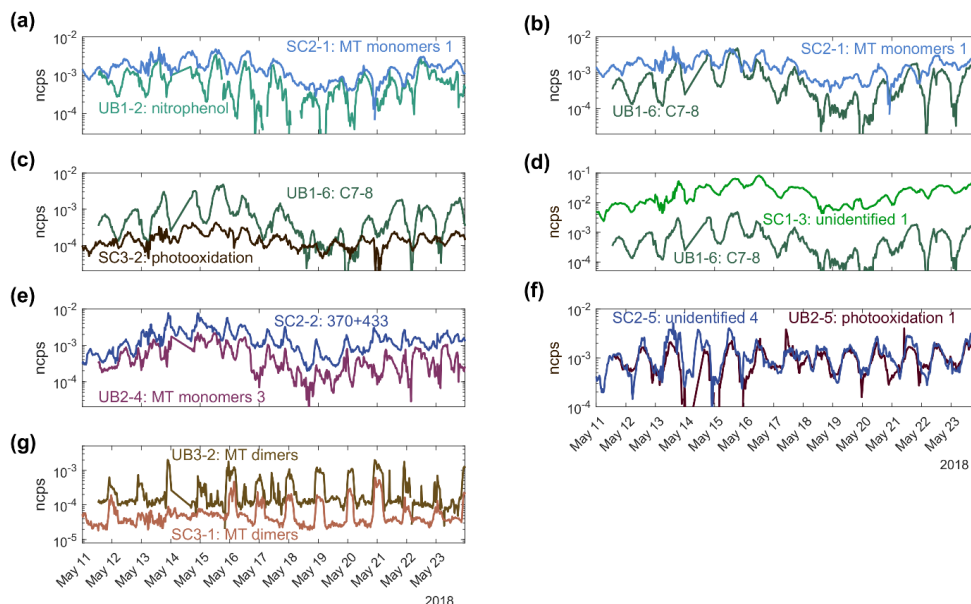
371 Tables 1 and S3 present the most plausible interpretation of selected and not selected factors, respectively. For each factor,  
372 we propose VOC precursors, oxidants, and terminators, which were most likely to influence the formation of species in  
373 this factor. We also specify an hour of the day when factor's signal reached its maximum as well as the contribution of  
374 this factor to the total signal both within its own m/Q sub-range and within the full analyzed range (200-650 Th). See  
375 Table 1 caption for a more detailed description of how to read the table. The findings and implications are discussed  
376 below.

377



378 Table 1. Suggested characterization of selected factors at both stations. Detailed factor interpretation is described in Sect.  
 379 S3. The importance of the various species described in this table was assessed based on either factor time series (TS),  
 380 factor mass spectra (MS), or both (B), as indicated by the superscript in the “Factor” column. The “Precursor” column  
 381 describes which type of molecules we expect to act as precursors to the observed signals, separating (when possible)  
 382 between AVOC and BVOC. The “Oxidant” and “Terminator” columns depict our estimates for the most likely species  
 383 involved in the oxidation process (“M”, as in “maybe”, is used if we were unable to exclude or confirm the participation  
 384 of the species). If the “yes” or “no” is marked in bold font, it means that we found a particularly clear influence of that  
 385 species for that factor. The “Diurnal peak time” shows the hour when the factor had its highest concentration, and  
 386 “Fraction” depicts the percentage of signal (of the given sub-range or the total analyzed m/Q range) that the factor  
 387 contributed to.

| Range [Th]                      | Factor              | Precursor                 | Oxidant    |                 |                | Terminator |                 |                 | Diurnal peak time | Fraction [%] within |           |
|---------------------------------|---------------------|---------------------------|------------|-----------------|----------------|------------|-----------------|-----------------|-------------------|---------------------|-----------|
|                                 |                     |                           | OH         | NO <sub>3</sub> | O <sub>3</sub> | NO         | RO <sub>2</sub> | HO <sub>2</sub> |                   | 200-650             | Sub-range |
| <b>Street canyon</b>            |                     |                           |            |                 |                |            |                 |                 |                   |                     |           |
| 350-500                         | SC2-1 <sup>TS</sup> | BVOCs                     | M          | no              | M              | yes        | no              | M               | 13                | 2.2                 | 27.2      |
|                                 | SC2-2 <sup>TS</sup> | VOCs                      | no         | <b>yes</b>      | M              | M          | no              | M               | 22                | 2.0                 | 24.8      |
|                                 | SC2-3 <sup>TS</sup> | BVOCs                     | no         | <b>yes</b>      | no             | no         | M               | M               | 0                 | 0.9                 | 11.5      |
| 500-650                         | SC3-1 <sup>B</sup>  | BVOCs                     | no         | yes             | no             | <b>no</b>  | yes             | no              | 22                | 0.1                 | 19.3      |
|                                 | SC3-2 <sup>MS</sup> | VOCs, noise, F-impurities | <b>yes</b> | no              | M              | yes        | no              | M               | 13                | 0.2                 | 41.6      |
| <b>Urban background station</b> |                     |                           |            |                 |                |            |                 |                 |                   |                     |           |
| 200-350                         | UB1-2 <sup>MS</sup> | AVOCs                     | <b>yes</b> | no              | no             | yes        | no              | M               | 12                | 8.9                 | 16.1      |
|                                 | UB1-6 <sup>TS</sup> | VOCs                      | M          | no              | M              | yes        | no              | M               | 17                | 7.4                 | 17.8      |
|                                 | UB2-1 <sup>TS</sup> | BVOCs                     | no         | <b>yes</b>      | no             | yes        | no              | M               | 21                | 2.6                 | 8.6       |
| 350-500                         | UB2-2 <sup>TS</sup> | BVOCs                     | no         | yes             | M              | <b>no</b>  | M               | M               | 21                | 5.4                 | 18.0      |
|                                 | UB2-3 <sup>MS</sup> | BVOCs                     | no         | yes             | M              | <b>no</b>  | no              | M               | 22                | 5.1                 | 17.0      |
|                                 | UB2-4 <sup>TS</sup> | BVOCs                     | M          | no              | M              | <b>yes</b> | no              | M               | 7                 | 4.9                 | 16.5      |
|                                 | UB2-5 <sup>MS</sup> | VOCs, noise               | <b>yes</b> | no              | M              | yes        | no              | M               | 12                | 12.0                | 39.9      |
| 500-650                         | UB3-1 <sup>B</sup>  | BVOCs                     | no         | yes             | M              | <b>no</b>  | no              | M               | 22                | 4.9                 | 34.3      |
|                                 | UB3-2 <sup>B</sup>  | BVOCs                     | no         | yes             | M              | <b>no</b>  | yes             | no              | 23                | 3.6                 | 25.4      |
|                                 | UB3-3 <sup>MS</sup> | VOCs, noise               | <b>yes</b> | no              | no             | yes        | no              | M               | 12                | 5.6                 | 40.3      |



388

389 Figure 5. Time series of PMF factors with Pearson correlation coefficient higher than 0.7 (Figure S9) between the street  
 390 canyon (SC) and the urban background station (UB) for common measurement time.

391 The total concentration of AVOCs is much higher than BVOCs at both stations (shown for street canyon in Fig. S8),  
 392 however, most of the selected factors are more likely to have biogenic origin, primarily based on the identified peaks in  
 393 the mass spectra (Table 1, Sect. S3). Our result is in agreement with the earlier study by Saarikoski et al. (2023) which  
 394 concluded that, despite dominant AVOCs concentrations at street canyon site, BVOCs are estimated to be the main source  
 395 of oxidized products, due to their higher reactivities. MT are the only type of biogenic precursors identified at the street  
 396 canyon while at the urban background station we find oxidation products of both MT and sesquiterpenes. This is likely  
 397 due to the difference in proximity of trees and vegetation from the stations as none of measured sesquiterpenes exceeded  
 398 0.2% of measured total BVOC concentrations at the street canyon. All key compounds detected in MT-derived factors  
 399 were previously reported in studies investigating the influence of NO<sub>x</sub> on HOM formation from MT precursors (Pullinen  
 400 et al., 2020; Yan et al., 2020; Shen et al., 2021; Dam et al., 2022; Guo et al., 2022a). Even though MT can be emitted  
 401 from anthropogenic sources, for instance in form of VCPs (Gkatzelis et al., 2021; Li et al., 2022), the population density  
 402 of Helsinki is low enough that that signature is likely lost among the abundant biogenic MT signals. This is in agreement  
 403 with  $\alpha$ -pinene being the most abundant BVOC and a common VCP, limonene (Coggon et al., 2021), being very low (<5%  
 404 of BVOC concentration).

405 We observed only few PMF factors that we expect to originate from AVOC oxidation, and for both stations AVOC factors  
 406 are detected only for the smallest m/Q sub-range, 200-350 Th (Table 1, Table S3). None of the factors had diurnal  
 407 variations resembling traffic emissions at these sites (Olin et al., 2020; Okuljar et al., 2021). Even though concentrations  
 408 of some factors differed between weekends and workdays, the diurnal behavior of factors was very similar (Fig. S12-13).  
 409 This suggests that the emissions from traffic at these sites did not oxidize to form HOM at adequate yields or time scales  
 410 to considerably contribute to our measured signals, in line with conclusions presented by Brean et al. (2019) and





411 Saarikoski et al. (2023). As precursor VOC concentrations are also affected by the mixing layer height (MLH), this effect  
412 may also impact HOM formation. However, VOCs are only one of the components that affect HOM formation, the effect  
413 of the MLH on HOM observed in this study is expected to be small.

414 Between the two stations, there are only a few factors with similar key compounds (Table S2). *SC3-1: MT dimers* has  
415 partly corresponding key compounds with *UB3-2: MT dimers*. They both contain  $C_{20}H_{32}O_xN_2$  compounds, where  $x$  is 11-  
416 15 for SC and 13-16 for UB. *UB3-2: MT dimers* contains also other types of dimers which are not usually present in *SC3-1: MT dimers*. These slight differences between stations may be caused by the small difference in concentration of oxidant,  
417 or the concentration or type of MT. The non-negligible concentration of NO during nighttime at SC may also impact the  
418 dimer formation there. Nevertheless, these factors are very similar and form through similar pathways (Table 1) –  
419 oxidation of MT mostly by  $NO_3$ , and termination through  $RO_2$  cross reactions, leading also to correlating time series  
420 ( $R=0.77$ ., Fig. 5 and S9). The  $RO_2 + RO_2$  reactions forming the MT-derived dimers will inevitably also form monomers  
421 as the dimer yield is never 100 %. However, monomers can also form through all other  $RO_2$  termination channels, making  
422 them much more heterogeneous than the dimers. The time evolution of some MT-derived monomer factor time series  
423 (*SC2-3: MT monomers 2* and *UB2-2: MT monomers 2*) correlate with the corresponding dimer factors ( $R= 0.71$  and  
424  $R=0.67$  respectively) as well as with each other ( $R=0.56$ ). While both factors are dominated by  $C_{10}$  compounds, their  
425 detailed mass spectra have significant differences (Fig. S2 and S3): *UB2-2: MT monomers 2* contains mainly ONCs with  
426 one N-atom while *SC2-3: MT monomers 2* has more compounds with two N-atoms (Table S2). This may indicate that  
427 there is enough NO available to terminate some fraction of the  $RO_2$ , yet without totally shutting down the  $RO_2 + RO_2$   
428 channel.  
429

430 Another pair of factors showing similarities between the stations is *SC2-2: 370+433* and *UB2-4: MT monomers 3* (Fig.  
431 5). Both factors are driven mostly by one compound ( $C_{10}H_{16}O_9N_2$ ), which has been detected as two clusters  
432  $C_{10}H_{16}O_9N_2 \cdot NO_3^-$  (370 Th) and  $C_{10}H_{16}O_9N_2 \cdot HNO_3 \cdot NO_3^-$  (433 Th) in our instrument (determined by correlation analysis).  
433 The high time series correlation ( $R=0.75$ ) suggests that molecules in these factors are formed via very similar pathways  
434 between the sites. Potentially, the formation pathways are identical, but importance of some competing pathways differ  
435 between the sites. Overall, the lack of stronger resemblance between these nearby sites suggests that even if HOM have  
436 the same VOC precursors, the environmental conditions regulate the relative importance between different oxidation  
437 pathways.

438 While differences in emissions and oxidation reactions will lead to diverse mass spectra, also the time series are expected  
439 to vary between the sites as the wind direction changes. For example, the street canyon site will likely be impacted by the  
440 street in different ways if the wind direction is from the street or towards the street. A clearly longer campaign than ours  
441 would be needed to identify the detailed impacts from different wind directions. However, analysis of the average diurnal  
442 variation can help us understand the roles of different oxidation conditions if the impact of varying wind directions  
443 diminishes in a longer average. Most factors at both stations can be characterized by one of a few types of diurnal patterns.  
444 Factors with a daytime diurnal variation reaching maximum concentration during noon or afternoon resemble diurnal  
445 variation of OH or  $O_3$ , respectively. However, temperature also peaks in the afternoon, and can lead to both higher BVOC  
446 emissions as well as evaporation of semi-volatile species from aerosols or surfaces, convoluting the effect of the oxidants  
447 on the observed HOM. Factors with noon or afternoon maxima are mostly found in range 1 at both sites, and to some  
448 extent in range 2. As these ranges mostly contain species thought to be semi-volatile (Peräkylä et al., 2020), it is possible  
449 that much of the observed variation is indeed due to the higher temperature causing increased partitioning of these



450 compounds into the gas phase. Nevertheless, OH and O<sub>3</sub> are likely involved as well, and given that the vast majority of  
451 signals are ONCs, RO<sub>2</sub> termination by NO is to be expected for most species. The opposite can be said for nighttime  
452 factors, which are likely inhibited in the daytime by NO, as their formation involves RO<sub>2</sub> termination via other pathways.  
453 This becomes especially visible for HOM terminated via RO<sub>2</sub> + RO<sub>2</sub> reactions (Ehn et al., 2014; Yan et al., 2016), which  
454 are mainly present in range 3. In this range, the volatilities are overwhelmingly low or extremely low, meaning that  
455 ambient temperature changes will not impact their ability to condense irreversibly to aerosols, thus also making their  
456 temporal behavior easier to interpret.

457 While daytime and nighttime peaks can be explained quite straightforwardly through variations in temperature or  
458 available oxidants or terminators that all follow distinct diurnal trends, we also observed additional types of diurnal trends,  
459 present mostly in range 2. Factor *UB2-1: Monoterpenes 1* had a peak in morning and evening (Fig. 4), around sunrise and  
460 sunset. We can speculate that these are the periods when sunlight was still available, but at limited amounts. This effect  
461 may cause an optimal situation for having both NO<sub>3</sub> and NO participating in the oxidation process. This is supported by  
462 the high N-atom content of the main species in this factor. Meanwhile, some other factors showed an opposite trend to  
463 UB2-1, namely minima during morning and evening, often with a strong nighttime peak and a smaller daytime increase.  
464 Some of the most prominent factors with such behavior were *SC2-3: MT monomers 2*, *UB2-2: MT monomers 2*, *UB2-3:*  
465 *sesquiterpene 1*, and *UB3-1: sesquiterpene 2*. NO<sub>3</sub> was identified as the main oxidant for these factors based on the mass  
466 spectra and the high nighttime signals, but the local maxima around noon is surprising. Saarikoski et al. (2023) did  
467 estimate that NO<sub>3</sub> would have a small daytime maximum, likely due to the sinks not being fast enough to fully overwhelm  
468 the very high formation rates from high O<sub>3</sub> and NO<sub>2</sub> during this time. We cannot determine to which extent the diurnal  
469 variation of NO<sub>3</sub> influences these diurnal patterns. As was the case also in many situations discussed above, we are often  
470 unable to separate if an increase is due to an enhanced source strength or a decrease in competing reaction pathways.

#### 471 **Comparison to previous research**

472 HOM data from Helsinki show similarities with previous studies done on ambient HOM data in urban as well as rural  
473 environments. Yan et al. (2016) investigated HOM formation pathways at a boreal forest site (SMEAR II station, Hyytiälä,  
474 Finland) located approximately 190 km from Helsinki and 50 km from the closest city – Tampere (with population  
475 approximately 250 000). A factor “*Nighttype type-2*”, obtained from PMF analysis by Yan et al. (2016) contained MT-  
476 derived dimers formed by NO<sub>3</sub> and O<sub>3</sub> oxidation and RO<sub>2</sub> termination. That factor mostly consisted of C<sub>20</sub>H<sub>31</sub>O<sub>10-18</sub>N  
477 (40%) and C<sub>20</sub>H<sub>32</sub>O<sub>10-17</sub>N<sub>2</sub> (20%) suggesting that the dimers detected in Hyytiälä and in Helsinki (both stations) have the  
478 same formation pathways, even though these measurement sites represent different rural and urban environment. Despite  
479 relatively similar precursors and formation pathways, far fewer similarities are found between the mass spectra of MT-  
480 derived monomer factors at these three sites. This suggests, as also mentioned above, that monomer formation pathways  
481 are much more diverse compared to dimer formation. Still, a comparison of our results with other studies done in rural  
482 environments (Massoli et al., 2018; Kürten et al., 2016) showed clearly lower resemblance between MT-derived dimers,  
483 which is likely a result of different biome types in their studies (isoprene-dominated south east US and rural agricultural  
484 site in Germany respectively) compared the ones conducted in Finland.

485 In recent years, more research on condensable vapor formation has been conducted in urban environments heavily  
486 influenced by NO<sub>x</sub> (Yan et al., 2022; Guo et al., 2022b; Liu et al., 2021; Nie et al., 2022; Zhang et al., 2022). Unlike forest  
487 environments, where the fraction of nitrogen-containing HOM is similar to the fraction of HOM without nitrogen atoms  
488 (Yan et al., 2016; Massoli et al., 2018), condensable vapor composition in Chinese megacities is dominated by nitrogen-



489 containing compounds, which represent approximately 60-85% of all measured condensable vapors (Guo et al., 2022b;  
490 Liu et al., 2021; Nie et al., 2022; Zhang et al., 2022). This strong influence by  $\text{NO}_x$  was also observed in the present  
491 study at both stations in Helsinki. In addition, the majority of key compounds in *SCI-5: nitrophenol & aliphatic* are also  
492 listed as main compounds in factors originating from aliphatic AVOCs detected in Nanjing (*Aliph-OOM*) (Liu et al.,  
493 2021) and in Beijing (*aliphatic OOMs*) (Guo et al., 2022b). However, depending on the time of the year, the main  
494 precursors for condensable vapors in cities in China are either AVOCs or a mix of AVOCs and BVOCs (Guo et al.,  
495 2022b; Liu et al., 2021; Nie et al., 2022). This is clearly different compared to Helsinki, where BVOC-derived vapors  
496 were more abundant. This dissimilarity is likely due to the AVOC:BVOC ratio being much larger in Chinese cities due  
497 to closer proximity of much larger areas with anthropogenic emissions. In contrast, Helsinki AVOC:BVOC is much  
498 smaller due to larger BVOC emissions from abundant vegetation in the close surroundings. It is also important to notice  
499 that most studies of condensable vapors in Chinese cities (Guo et al., 2022b; Liu et al., 2021; Nie et al., 2022) analyzed  
500 much smaller mass range (200-400 Th or 250-400 Th), which corresponds to range 1-2 here. In our study, range 1 is the  
501 only mass range in which we find the dominant influence of anthropogenic precursors. Brean et al. (2019) also showed  
502 that MT-derived dimer concentrations were approximately 50 times lower than MT-derived monomers in Beijing, likely  
503 due to both small MT emissions and suppression of dimer formation by  $\text{NO}$ .

### 504 3.3. Implications for air quality

505 Ambient air pollution was recognized as the largest environmental health risk and one of the top risk factors for the loss  
506 of healthy years (Lim et al., 2012; Anderson et al., 2012; Cohen et al., 2017). Premature deaths caused by ambient air  
507 pollution are linked to particular matter (PM) (Cohen et al., 2017; WHO, 2021), both due to short-term (Pope and Dockery,  
508 2012) and long-term exposure (Burnett et al., 2014). In many environments, including different urban areas, PM is  
509 dominated by secondary aerosol formed from condensable vapors, including HOM. HOM and other condensable organic  
510 vapors impact not only PM concentration but also the chemical composition of SOA and, consequently, aerosol properties  
511 like toxicity. For example, in a recent study with human alveolar epithelial cells and human monocyte cells, the organic  
512 compounds and the aging of the aerosol were major drivers of the cell level toxicity of aerosol (Hakkarainen et al., 2022).

513 In this work, we found that the majority of low-volatility condensable vapors in Helsinki were impacted by both biogenic  
514 and anthropogenic precursors, despite high local anthropogenic emissions. The VOC precursors themselves were mostly  
515 of biogenic origin, i.e. BVOC, but the oxidation process was strongly perturbed by anthropogenic activity, particularly  
516 by  $\text{NO}_x$ . While detailed similarities in mass spectra of factors were often small between the close-by sites studied here,  
517 most observed compounds at both stations were ONCs. Previous studies have shown that  $\text{NO}_x$  can change the yield of  
518 SOA formation during VOC oxidation (Mutzel et al., 2021; Jaoui et al., 2013; Ng et al., 2017), though this effect may be  
519 not as clear to observe in ambient measurements (Yan et al., 2022). In the smaller m/Q ranges studied in this work, the  
520 influence from AVOC was larger, but we cannot deduce the impact of these factors on SOA formation due to their semi-  
521 volatile nature. Nevertheless, our results indicate that in Helsinki, and likely in other biologically influenced urban areas,  
522 anthropogenic emissions affect HOM formation and composition most strongly by the participation of  $\text{NO}_x$  in the (B)VOC  
523 oxidation. That influence will be propagated to the SOA, both concerning the composition as well as the effective yield  
524 of SOA from the BVOC oxidation, but quantifying the ultimate impact on either of these will require further studies.

### 525 4. Conclusions



526 We measured the composition of condensable vapors, HOM, during late spring at two stations separated by 900 m in  
527 different sub-environments in Helsinki, a city with considerable biogenic influence from trees. We compared HOM  
528 composition and formation pathways at the two sites, an urban background station and a street canyon, using PMF analysis  
529 to separate the complex data into covarying compound groups. We found that the majority of the HOM originated from  
530 BVOCs at both locations, despite them being dominated by AVOC emissions (Rantala et al., 2016; Saarikoski et al.,  
531 2023). However, we did observe a strong anthropogenic influence on the HOM formation, due to the elevated  $\text{NO}_x$   
532 concentrations at both stations, which is consistent with previous studies conducted in urban environments (Guo et al.,  
533 2022b; Liu et al., 2021; Nie et al., 2022). The PMF factors, and their temporal behavior, were surprisingly different  
534 between the two sites, considering their relatively close proximity. Monoterpene-derived dimers were the compound  
535 groups that correlated best between the sites. On the contrary, at the street canyon site we observed a factor corresponding  
536 partly to AVOC-derived factors found in Chinese megacities (Guo et al., 2022b; Liu et al., 2021; Nie et al., 2022). The  
537 lack of a similar factor in the PMF solution from the urban background station highlights that HOM composition at two  
538 nearby sites in an urban environment can differ noticeably depending on the local anthropogenic influences. To a large  
539 extent, we expect this difference to be driven by differences in the environmental conditions, leading to distinct oxidation  
540 products even when the same VOC molecule becomes oxidized, due to competition between both oxidants and  $\text{RO}_2$   
541 terminators.

542 Our work indicates that when analyzing and discussing the impact of HOM on SOA and air quality in urban environments,  
543 we need to keep in mind the spatial inhomogeneity of urban areas in the HOM composition and formation mechanisms.  
544 Thus, a more detailed investigation of the formation and composition of HOM in a variety of different urban sub-  
545 environments would be beneficial. Additionally, our findings are restricted to a short and biologically active period, hence  
546 follow-up research on seasonal changes is needed. Finally, we recommend that future mass spectrometric studies in urban  
547 area employ devices with resolving power above 5000 Th/Th, as the mass spectra are extremely complex and thus even  
548 peak identification can be a major challenge.

#### 549 **Data availability**

550 All data presented in this manuscript will be available in open repository before the final version of manuscript is  
551 completed.

#### 552 **Author contribution**

553 The main ideas were formulated by OG, HT, JKo, JVM, MS, MDM TR, TP, MK and the results were interpreted by  
554 MOk, OG, PP, and ME. TR, HK, OG, HT prepared measurement methodology and OG, MOI, JKa, HH, and HK  
555 contributed to data collection. MOk performed the data analysis and YZ supported it. OG and EH supervised the project.  
556 HT, MDM, and TP made a funding acquisition. MOk visualized data and prepared the manuscript with contributions  
557 from OG, ME. All the authors reviewed and commented the manuscript.

#### 558 **Competing interests**

559 The authors declare that they have no conflict of interest.

#### 560 **Acknowledgments.**



561 This research was supported by the Regional innovations and experimentations funds AIKO (project HAQT, AIKO014),  
562 Business Finland (CITYZER project, Tekes nro: 3021/31/2015 and 2883/31/2015), Pegasor Oy and HSY, Academy of  
563 Finland (grant nos 273010, 307331, 310626, 311932, 318940, 1325656, 326437, and ACCC flagship grant no. 337549,  
564 337552, 337551), Healthy Outdoor Premises for Everyone (HOPE), Urban Innovation Actions, Regional development  
565 funds, The Technology Industries of Finland Centennial Foundation via project *Urbaani ilmanlaatu 2.0*, European  
566 Commission via Horizon Europe project “Non-CO2 Forcers and their Climate, Weather, Air Quality and Health Impacts,  
567 FOCl” (101056783), Faculty of Science 3-year grant (75284132), Tampere University of Technology graduate school,  
568 European Research Council (ERC) project ADAPT (grant no. 101002728), European Union Horizon 2020 research and  
569 innovation programme (grant no 101036245, RI-URBANS; grant no. 821205, FORCeS, and ERA-PLANET project  
570 SMURBS, 689443).

571 We would like to thank the people who took care of instruments and helped with measurements at the SMEAR III (Pekka  
572 Rantala, Erkki Siivola, Pasi Aalto, Petri Keronen, Frans Korhonen, Tiia Laurila, Lauriane Quéléver, Tuuli Lehmusjärvi,  
573 Deniz Kemppainen) and the HSY Mäkelänkatu site (Anssi Julkunen, Anders Svens, Harri Portin, Taneli Mäkelä, Tommi  
574 Wallenius, Anu Kousa).

#### 575 References

576 Anderson, J. O., Thundiyil, J. G., and Stolbach, A.: Clearing the Air: A Review of the Effects of Particulate Matter Air  
577 Pollution on Human Health, *J. Med. Toxicol.*, 8, 166–175, <https://doi.org/10.1007/S13181-011-0203-1/TABLES/5>,  
578 2012.

579 Atkinson, R. and Arey, J.: Atmospheric degradation of volatile organic compounds, *Chem. Rev.*, 103, 4605–4638,  
580 <https://doi.org/10.1021/CR0206420>, 2003.

581 Bianchi, F., Garmash, O., He, X., Yan, C., Iyer, S., Rosendahl, I., Xu, Z., Rissanen, M. P., Riva, M., Taipale, R.,  
582 Sarnela, N., Petäjä, T., Worsnop, D. R., Kulmala, M., Ehn, M., and Junninen, H.: The role of highly oxygenated  
583 molecules (HOMs) in determining the composition of ambient ions in the boreal forest, *Atmos. Chem. Phys.*, 17,  
584 13819–13831, <https://doi.org/10.5194/ACP-17-13819-2017>, 2017.

585 Bianchi, F., Kurtén, T., Riva, M., Mohr, C., Rissanen, M. P., Roldin, P., Berndt, T., Crouse, J. D., Wennberg, P. O.,  
586 Mentel, T. F., Wildt, J., Junninen, H., Jokinen, T., Kulmala, M., Worsnop, D. R., Thornton, J. A., Donahue, N.,  
587 Kjaergaard, H. G., and Ehn, M.: Highly Oxygenated Organic Molecules (HOM) from Gas-Phase Autoxidation  
588 Involving Peroxy Radicals: A Key Contributor to Atmospheric Aerosol, *Chem. Rev.*, 119, 3472–3509,  
589 <https://doi.org/10.1021/ACS.CHEMREV.8B00395>, 2019.

590 Brean, J., Harrison, R. M., Shi, Z., Beddows, D. C. S., Acton, W. J. F., Nicholas Hewitt, C., Squires, F. A., and Lee, J.:  
591 Observations of highly oxidized molecules and particle nucleation in the atmosphere of Beijing, *Atmos. Chem. Phys.*,  
592 19, 14933–14947, <https://doi.org/10.5194/ACP-19-14933-2019>, 2019.

593 Burnett, R. T., Arden Pope, C., Ezzati, M., Olives, C., Lim, S. S., Mehta, S., Shin, H. H., Singh, G., Hubbell, B.,  
594 Brauer, M., Ross Anderson, H., Smith, K. R., Balmes, J. R., Bruce, N. G., Kan, H., Laden, F., Prüss-Ustün, A., Turner,  
595 M. C., Gapstur, S. M., Diver, W. R., and Cohen, A.: An Integrated Risk Function for Estimating the Global Burden of  
596 Disease Attributable to Ambient Fine Particulate Matter Exposure, *Environ. Health Perspect.*, 122, 397–403,  
597 <https://doi.org/10.1289/EHP.1307049>, 2014.



- 598 Canonaco, F., Crippa, M., Slowik, J. G., Baltensperger, U., and Prévôt, A. S. H.: SoFi, an IGOR-based interface for the  
599 efficient use of the generalized multilinear engine (ME-2) for the source apportionment: ME-2 application to aerosol  
600 mass spectrometer data, *Atmos. Meas. Tech.*, 6, 3649–3661, <https://doi.org/10.5194/AMT-6-3649-2013>, 2013.
- 601 Chen, G., Canonaco, F., Tobler, A., Aas, W., Alastuey, A., Allan, J., Atabakhsh, S., Aurela, M., Baltensperger, U.,  
602 Bougiatioti, A., De Brito, J. F., Ceburnis, D., Chazeanu, B., Chebaicheb, H., Daellenbach, K. R., Ehn, M., El Haddad, I.,  
603 Eleftheriadis, K., Favez, O., Flentje, H., Font, A., Fossum, K., Freney, E., Gini, M., Green, D. C., Heikkinen, L.,  
604 Herrmann, H., Kalogridis, A. C., Keernik, H., Lhotka, R., Lin, C., Lunder, C., Maasikmets, M., Manousakas, M. I.,  
605 Marchand, N., Marin, C., Marmureanu, L., Mihalopoulos, N., Močnik, G., Nečki, J., O’Dowd, C., Ovadnevaite, J.,  
606 Peter, T., Petit, J. E., Pikridas, M., Matthew Platt, S., Pokorná, P., Poulain, L., Priestman, M., Riffault, V., Rinaldi, M.,  
607 Róžański, K., Schwarz, J., Sciare, J., Simon, L., Skiba, A., Slowik, J. G., Sosedova, Y., Stavroulas, I., Styszko, K.,  
608 Teinemaa, E., Timonen, H., Tremper, A., Vasilescu, J., Via, M., Vodička, P., Wiedensohler, A., Zografou, O., Cruz  
609 Mingüillón, M., and Prévôt, A. S. H.: European aerosol phenomenology – 8: Harmonised source apportionment of  
610 organic aerosol using 22 Year-long ACSM/AMS datasets, *Environ. Int.*, 166, 107325,  
611 <https://doi.org/10.1016/J.ENVINT.2022.107325>, 2022.
- 612 Coggon, M. M., Gkatzelis, G. I., McDonald, B. C., Gilman, J. B., Schwantes, R. H., Abuhassan, N., Aikin, K. C.,  
613 Arendt, M. F., Berkoff, T. A., Brown, S. S., Campos, T. L., Dickerson, R. R., Gronoff, G., Hurley, J. F., Isaacman-  
614 Vanwertz, G., Koss, A. R., Li, M., McKeen, S. A., Moshary, F., Peischl, J., Pospisilova, V., Ren, X., Wilson, A., Wu,  
615 Y., Trainer, M., and Warneke, C.: Volatile chemical product emissions enhance ozone and modulate urban chemistry,  
616 *Proc. Natl. Acad. Sci. U. S. A.*, 118, e2026653118,  
617 [https://doi.org/10.1073/PNAS.2026653118/SUPPL\\_FILE/PNAS.2026653118.SAPP.PDF](https://doi.org/10.1073/PNAS.2026653118/SUPPL_FILE/PNAS.2026653118.SAPP.PDF), 2021.
- 618 Cohen, A. J., Brauer, M., Burnett, R., Anderson, H. R., Frostad, J., Estep, K., Balakrishnan, K., Brunekreef, B.,  
619 Dandona, L., Dandona, R., Feigin, V., Freedman, G., Hubbell, B., Jobling, A., Kan, H., Knibbs, L., Liu, Y., Martin, R.,  
620 Morawska, L., Pope, C. A., Shin, H., Straif, K., Shaddick, G., Thomas, M., van Dingenen, R., van Donkelaar, A., Vos,  
621 T., Murray, C. J. L., and Forouzanfar, M. H.: Estimates and 25-year trends of the global burden of disease attributable  
622 to ambient air pollution: an analysis of data from the Global Burden of Diseases Study 2015, *Lancet*, 389, 1907–1918,  
623 [https://doi.org/10.1016/S0140-6736\(17\)30505-6](https://doi.org/10.1016/S0140-6736(17)30505-6), 2017.
- 624 Crounse, J. D., Nielsen, L. B., Jørgensen, S., Kjaergaard, H. G., and Wennberg, P. O.: Autoxidation of organic  
625 compounds in the atmosphere, *J. Phys. Chem. Lett.*, 4, 3513–3520,  
626 [https://doi.org/10.1021/JZ4019207/SUPPL\\_FILE/JZ4019207\\_SI\\_001.PDF](https://doi.org/10.1021/JZ4019207/SUPPL_FILE/JZ4019207_SI_001.PDF), 2013.
- 627 Crutzen, P. J., Lawrence, M. G., and Pöschl, U.: On the background photochemistry of tropospheric ozone, *Tellus, Ser.*  
628 *B Chem. Phys. Meteorol.*, 51, 123–146, <https://doi.org/10.1034/J.1600-0889.1999.00010.X>, 1999.
- 629 Dam, M., Draper, D. C., Marsavin, A., Fry, J. L., and Smith, J. N.: Observations of gas-phase products from the nitrate-  
630 radical-initiated oxidation of four monoterpenes, *Atmos. Chem. Phys.*, 22, 9017–9031, [https://doi.org/10.5194/ACP-22-](https://doi.org/10.5194/ACP-22-9017-2022)  
631 [9017-2022](https://doi.org/10.5194/ACP-22-9017-2022), 2022.
- 632 Ehn, M., Thornton, J. A., Kleist, E., Sipilä, M., Junninen, H., Pullinen, I., Springer, M., Rubach, F., Tillmann, R., Lee,  
633 B., Lopez-Hilfiker, F., Andres, S., Acir, I. H., Rissanen, M., Jokinen, T., Schobesberger, S., Kangasluoma, J.,  
634 Kontkanen, J., Nieminen, T., Kurtén, T., Nielsen, L. B., Jørgensen, S., Kjaergaard, H. G., Canagaratna, M., Maso, M.





- 635 D., Berndt, T., Petäjä, T., Wahner, A., Kerminen, V. M., Kulmala, M., Worsnop, D. R., Wildt, J., and Mentel, T. F.: A  
636 large source of low-volatility secondary organic aerosol, *Nature*, 506, 476–479, <https://doi.org/10.1038/nature13032>,  
637 2014.
- 638 Fry, J. L., Draper, D. C., Barsanti, K. C., Smith, J. N., Ortega, J., Winkler, P. M., Lawler, M. J., Brown, S. S., Edwards,  
639 P. M., Cohen, R. C., and Lee, L.: Secondary organic aerosol formation and organic nitrate yield from NO<sub>3</sub> oxidation of  
640 biogenic hydrocarbons, *Environ. Sci. Technol.*, 48, 11944–11953,  
641 [https://doi.org/10.1021/ES502204X/SUPPL\\_FILE/ES502204X\\_SI\\_001.PDF](https://doi.org/10.1021/ES502204X/SUPPL_FILE/ES502204X_SI_001.PDF), 2014.
- 642 Garmash, O., Rissanen, M. P., Pullinen, I., Schmitt, S., Kausiala, O., Tillmann, R., Zhao, D., Percival, C., Bannan, T. J.,  
643 Priestley, M., Hallquist, Å. M., Kleist, E., Kiendler-Scharr, A., Hallquist, M., Berndt, T., McFiggans, G., Wildt, J. J.,  
644 Mentel, T. F., Ehn, M., Hallquist, A. M., Kleist, E., Kiendler-Scharr, A., Hallquist, M., Berndt, T., McFiggans, G.,  
645 Wildt, J. J., Mentel, T. F., and Ehn, M.: Multi-generation OH oxidation as a source for highly oxygenated organic  
646 molecules from aromatics, *Atmos. Chem. Phys.*, 20, 515–537, <https://doi.org/10.5194/acp-20-515-2020>, 2020.
- 647 Gkatzelis, G. I., Coggon, M. M., McDonald, B. C., Peischl, J., Gilman, J. B., Aikin, K. C., Robinson, M. A., Canonaco,  
648 F., Prevot, A. S. H., Trainer, M., and Warneke, C.: Observations Confirm that Volatile Chemical Products Are a Major  
649 Source of Petrochemical Emissions in U.S. Cities, *Environ. Sci. Technol.*, 55, 4332–4343,  
650 [https://doi.org/10.1021/ACS.EST.0C05471/ASSET/IMAGES/LARGE/ES0C05471\\_0005.JPEG](https://doi.org/10.1021/ACS.EST.0C05471/ASSET/IMAGES/LARGE/ES0C05471_0005.JPEG), 2021.
- 651 Guo, Y., Shen, H., Pullinen, I., Luo, H., Kang, S., Vereecken, L., Fuchs, H., Hallquist, M., Acir, I. H., Tillmann, R.,  
652 Rohrer, F., Wildt, J., Kiendler-Scharr, A., Wahner, A., Zhao, D., and Mentel, T. F.: Identification of highly oxygenated  
653 organic molecules and their role in aerosol formation in the reaction of limonene with nitrate radical, *Atmos. Chem.*  
654 *Phys.*, 22, 11323–11346, <https://doi.org/10.5194/ACP-22-11323-2022>, 2022a.
- 655 Guo, Y., Yan, C., Liu, Y., Qiao, X., Zheng, F., Zhang, Y., Zhou, Y., Li, C., Fan, X., Lin, Z., Feng, Z., Zhang, Y.,  
656 Zheng, P., Tian, L., Nie, W., Wang, Z., Huang, D., Daellenbach, K. R., Yao, L., Dada, L., Bianchi, F., Jiang, J., Liu, Y.,  
657 Kerminen, V. M., and Kulmala, M.: Seasonal variation in oxygenated organic molecules in urban Beijing and their  
658 contribution to secondary organic aerosol, *Atmos. Chem. Phys.*, 22, 10077–10097, [https://doi.org/10.5194/ACP-22-](https://doi.org/10.5194/ACP-22-10077-2022)  
659 10077-2022, 2022b.
- 660 Hakkarainen, H., Salo, L., Mikkonen, S., Saarikoski, S., Aurela, M., Teinilä, K., Ihalainen, M., Martikainen, S.,  
661 Marjanen, P., Lepistö, T., Kuittinen, N., Saarnio, K., Aakko-Saksa, P., Pfeiffer, T. V., Timonen, H., Rönkkö, T., and  
662 Jalava, P. I.: Black carbon toxicity dependence on particle coating: Measurements with a novel cell exposure method,  
663 *Sci. Total Environ.*, 838, 156543, <https://doi.org/10.1016/J.SCITOTENV.2022.156543>, 2022.
- 664 Helin, A., Hakola, H., and Hellén, H.: Optimisation of a thermal desorption-gas chromatography-mass spectrometry  
665 method for the analysis of monoterpenes, sesquiterpenes and diterpenes, *Atmos. Meas. Tech.*, 13, 3543–3560,  
666 <https://doi.org/10.5194/AMT-13-3543-2020>, 2020.
- 667 Hyttinen, N., Kupiainen-Määttä, O., Rissanen, M. P., Muuronen, M., Ehn, M., and Kurtén, T.: Modeling the Charging  
668 of Highly Oxidized Cyclohexene Ozonolysis Products Using Nitrate-Based Chemical Ionization, *J. Phys. Chem. A*,  
669 119, 6339–6345, [https://doi.org/10.1021/ACS.JPCA.5B01818/SUPPL\\_FILE/JP5B01818\\_SI\\_001.PDF](https://doi.org/10.1021/ACS.JPCA.5B01818/SUPPL_FILE/JP5B01818_SI_001.PDF), 2015.
- 670 Jaoui, M., Kleindienst, T. E., Docherty, K. S., Lewandowski, M., Offenberg, J. H., Jaoui, M., Kleindienst, T. E.,



- 671 Docherty, K. S., Lewandowski, M., and Offenberg, J. H.: Secondary organic aerosol formation from the oxidation of a  
672 series of sesquiterpenes:  $\alpha$ -cedrene,  $\beta$ -caryophyllene,  $\alpha$ -humulene and  $\alpha$ -farnesene with O<sub>3</sub>, OH and NO<sub>3</sub> radicals,  
673 *Environ. Chem.*, 10, 178–193, <https://doi.org/10.1071/EN13025>, 2013.
- 674 Järvi, L., Hannuniemi, H., Hussein, T., Junninen, H., Aalto, P. P., Hillamo, R., Mäkelä, T., Keronen, P., Siivola, E.,  
675 Vesala, T., and Kulmala, M.: The urban measurement station SMEAR III: Continuous monitoring of air pollution and  
676 surface-atmosphere interactions in Helsinki, Finland, *Boreal Environ. Res.*, 14, 86–109, 2009.
- 677 Jokinen, T., Sipilä, M., Junninen, H., Ehn, M., Lönn, G., Hakala, J., Petäjä, T., Mauldin, R. L., Kulmala, M., Worsnop,  
678 D. R., Mauldin III, R. L., Kulmala, M., and Worsnop, D. R.: Atmospheric sulphuric acid and neutral cluster  
679 measurements using CI-API-TOF, *Atmos. Chem. Phys.*, 12, 4117–4125, <https://doi.org/10.5194/acp-12-4117-2012>,  
680 2012.
- 681 Junninen, H., Ehn, M., Petäjä, T., Luosujärvi, L., Kotiaho, T., Kostianen, R., Rohner, U., Gonin, M., Fuhrer, K.,  
682 Kulmala, M., and Worsnop, D. R.: A high-resolution mass spectrometer to measure atmospheric ion composition,  
683 *Atmos. Meas. Tech.*, 3, 1039–1053, <https://doi.org/10.5194/amt-3-1039-2010>, 2010.
- 684 Koppmann, R.: Anthropogenic VOCs, in: *Volatile Organic Compounds in the Atmosphere*, 2007.
- 685 Kroll, J. H. and Seinfeld, J. H.: Chemistry of secondary organic aerosol: Formation and evolution of low-volatility  
686 organics in the atmosphere, *Atmos. Environ.*, 42, 3593–3624, <https://doi.org/10.1016/J.ATMOENV.2008.01.003>,  
687 2008.
- 688 Kürten, A., Bergen, A., Heinritzi, M., Leiminger, M., Lorenz, V., Piel, F., Simon, M., Sitals, R., Wagner, A. C., and  
689 Curtius, J.: Observation of new particle formation and measurement of sulfuric acid, ammonia, amines and highly  
690 oxidized organic molecules at a rural site in central Germany, *Atmos. Chem. Phys.*, 16, 12793–12813,  
691 <https://doi.org/10.5194/acp-16-12793-2016>, 2016.
- 692 Kuuluvainen, H., Poikkimäki, M., Järvinen, A., Kuula, J., Irjala, M., Dal Maso, M., Keskinen, J., Timonen, H., Niemi,  
693 J. V., and Rönkkö, T.: Vertical profiles of lung deposited surface area concentration of particulate matter measured with  
694 a drone in a street canyon, *Environ. Pollut.*, 241, 96–105, <https://doi.org/10.1016/j.envpol.2018.04.100>, 2018.
- 695 Li, X.-B., Yuan, B., Wang, S., Wang, C., Lan, J., Liu, Z., Song, Y., He, X., Huangfu, Y., Pei, C., Cheng, P., Yang, S.,  
696 Qi, J., Wu, C., Huang, S., You, Y., Chang, M., Zheng, H., Yang, W., Wang, X., and Shao, M.: Variations and sources  
697 of volatile organic compounds (VOCs) in urban region: insights from measurements on a tall tower, *Atmos. Chem.*  
698 *Phys.*, 22, 10567–10587, <https://doi.org/10.5194/acp-22-10567-2022>, 2022.
- 699 Lim, S. S., Vos, T., Flaxman, A. D., Danaei, G., Shibuya, K., Adair-Rohani, H., Amann, M., Anderson, H. R., Andrews,  
700 K. G., Aryee, M., Atkinson, C., Bacchus, L. J., Bahalim, A. N., Balakrishnan, K., Balmes, J., Barker-Collo, S., Baxter,  
701 A., Bell, M. L., Blore, J. D., Blyth, F., Bonner, C., Borges, G., Bourne, R., Boussinesq, M., Brauer, M., Brooks, P.,  
702 Bruce, N. G., Brunekreef, B., Bryan-Hancock, C., Bucello, C., Buchbinder, R., Bull, F., Burnett, R. T., Byers, T. E.,  
703 Calabria, B., Carapetis, J., Carnahan, E., Chafe, Z., Charlson, F., Chen, H., Chen, J. S., Cheng, A. T. A., Child, J. C.,  
704 Cohen, A., Colson, K. E., Cowie, B. C., Darby, S., Darling, S., Davis, A., Degenhardt, L., Dentener, F., Des Jarlais, D.  
705 C., Devries, K., Dherani, M., Ding, E. L., Dorsey, E. R., Driscoll, T., Edmond, K., Ali, S. E., Engell, R. E., Erwin, P. J.,  
706 Fahimi, S., Falder, G., Farzadfar, F., Ferrari, A., Finucane, M. M., Flaxman, S., Fowkes, F. G. R., Freedman, G.,



- 707 Freeman, M. K., Gakidou, E., Ghosh, S., Giovannucci, E., Gmel, G., Graham, K., Grainger, R., Grant, B., Gunnell, D.,  
708 Gutierrez, H. R., Hall, W., Hoek, H. W., Hogan, A., Hosgood, H. D., Hoy, D., Hu, H., Hubbell, B. J., Hutchings, S. J.,  
709 Ibeanusi, S. E., Jacklyn, G. L., Jasrasaria, R., Jonas, J. B., Kan, H., Kanis, J. A., Kassebaum, N., Kawakami, N., Khang,  
710 Y. H., Khatibzadeh, S., Khoo, J. P., Kok, C., et al.: A comparative risk assessment of burden of disease and injury  
711 attributable to 67 risk factors and risk factor clusters in 21 regions, 1990-2010: A systematic analysis for the Global  
712 Burden of Disease Study 2010, *Lancet*, 380, 2224–2260, [https://doi.org/10.1016/S0140-6736\(12\)61766-8](https://doi.org/10.1016/S0140-6736(12)61766-8), 2012.
- 713 Liu, S. C., Kley, D., McFarland, M., Mahlman, J. D., and Levy, H.: On the origin of tropospheric ozone., *J. Geophys.*  
714 *Res.*, 85, 7546–7552, <https://doi.org/10.1029/JC0851C12P07546>, 1980.
- 715 Liu, Y., Nie, W., Li, Y., Ge, D., Liu, C., Xu, Z., Chen, L., Wang, T., Wang, L., Sun, P., Qi, X., Wang, J., Xu, Z., Yuan,  
716 J., Yan, C., Zhang, Y., Huang, D., Wang, Z., Donahue, N. M., Worsnop, D., Chi, X., Ehn, M., and DIng, A.: Formation  
717 of condensable organic vapors from anthropogenic and biogenic volatile organic compounds (VOCs) is strongly  
718 perturbed by NO<sub>x</sub> in eastern China, *Atmos. Chem. Phys.*, 21, 14789–14814, [https://doi.org/10.5194/ACP-21-14789-](https://doi.org/10.5194/ACP-21-14789-2021)  
719 2021, 2021.
- 720 Massoli, P., Stark, H., Canagaratna, M. R., Krechmer, J. E., Xu, L., Ng, N. L., Mauldin, R. L., Yan, C., Kimmel, J.,  
721 Misztal, P. K., Jimenez, J. L., Jayne, J. T., and Worsnop, D. R.: Ambient Measurements of Highly Oxidized Gas-Phase  
722 Molecules during the Southern Oxidant and Aerosol Study (SOAS) 2013, *ACS Earth Sp. Chem.*, 2, 653–672,  
723 <https://doi.org/10.1021/acsearthspacechem.8b00028>, 2018.
- 724 McDonald, B. C., De Gouw, J. A., Gilman, J. B., Jathar, S. H., Akherati, A., Cappa, C. D., Jimenez, J. L., Lee-Taylor,  
725 J., Hayes, P. L., McKeen, S. A., Cui, Y. Y., Kim, S. W., Gentner, D. R., Isaacman-VanWertz, G., Goldstein, A. H.,  
726 Harley, R. A., Frost, G. J., Roberts, J. M., Ryerson, T. B., and Trainer, M.: Volatile chemical products emerging as  
727 largest petrochemical source of urban organic emissions, *Science* (80-. ), 359, 760–764,  
728 [https://doi.org/10.1126/SCIENCE.AAQ0524/SUPPL\\_FILE/AAQ0524\\_MCDONALD\\_SM.PDF](https://doi.org/10.1126/SCIENCE.AAQ0524/SUPPL_FILE/AAQ0524_MCDONALD_SM.PDF), 2018.
- 729 Molteni, U., Bianchi, F., Klein, F., El Haddad, I., Frege, C., Rossi, M. J., Dommen, J., and Baltensperger, U.: Formation  
730 of highly oxygenated organic molecules from aromatic compounds, *Atmos. Chem. Phys.*, 18, 1909–1921,  
731 <https://doi.org/10.5194/acp-18-1909-2018>, 2018.
- 732 Mutzel, A., Zhang, Y., Böge, O., Rodigast, M., Kolodziejczyk, A., Wang, X., and Herrmann, H.: Importance of  
733 secondary organic aerosol formation of  $\alpha$ / $i$ -pinene, limonene, and  $m$ / $i$ -cresol comparing day- And nighttime radical  
734 chemistry, *Atmos. Chem. Phys.*, 21, 8479–8498, <https://doi.org/10.5194/ACP-21-8479-2021>, 2021.
- 735 Ng, N. L., Herndon, S. C., Trimborn, A., Canagaratna, M. R., Croteau, P. L., Onasch, T. B., Sueper, D., Worsnop, D.  
736 R., Zhang, Q., Sun, Y. L., and Jayne, J. T.: An Aerosol Chemical Speciation Monitor (ACSM) for Routine Monitoring  
737 of the Composition and Mass Concentrations of Ambient Aerosol, 45, 780–794,  
738 <https://doi.org/10.1080/02786826.2011.560211>, 2011.
- 739 Ng, N. L., Brown, S. S., Archibald, A. T., Atlas, E., Cohen, R. C., Crowley, J. N., Day, D. A., Donahue, N. M., Fry, J.  
740 L., Fuchs, H., Griffin, R. J., Guzman, M. I., Herrmann, H., Hodzic, A., Iinuma, Y., Jimenez, J. L., Kiendler-Scharr, A.,  
741 Lee, B. H., Luecken, D. J., Mao, J., McLaren, R., Mutzel, A., Osthoff, H. D., Picquet-Varrault, B., Platt, U., Pye, H. O.  
742 T., Rudich, Y., Schwantes, R. H., Shiraiwa, M., Stutz, J., Thornton, J. A., Tilgner, A., Williams, B. J., and Zaveri, R.  
743 A.: Nitrate radicals and biogenic volatile organic compounds: oxidation, mechanisms, and organic aerosol, *Atmos.*



- 744 Chem. Phys., 17, 2103–2162, <https://doi.org/10.5194/acp-17-2103-2017>, 2017.
- 745 Nie, W., Yan, C., Huang, D. D., Wang, Z., Liu, Y., Qiao, X., Guo, Y., Tian, L., Zheng, P., Xu, Z., Li, Y., Xu, Z., Qi, X.,  
746 Sun, P., Wang, J., Zheng, F., Li, X., Yin, R., Dallenbach, K. R., Bianchi, F., Petäjä, T., Zhang, Y., Wang, M., Schervish,  
747 M., Wang, S., Qiao, L., Wang, Q., Zhou, M., Wang, H., Yu, C., Yao, D., Guo, H., Ye, P., Lee, S., Li, Y. J., Liu, Y., Chi,  
748 X., Kerminen, V.-M., Ehn, M., Donahue, N. M., Wang, T., Huang, C., Kulmala, M., Worsnop, D., Jiang, J., and Ding,  
749 A.: Secondary organic aerosol formed by condensing anthropogenic vapours over China’s megacities, *Nat. Geosci.*  
750 2022, 1–7, <https://doi.org/10.1038/s41561-022-00922-5>, 2022.
- 751 Okuljar, M., Kuuluvainen, H., Kontkanen, J., Garmash, O., Olin, M., Niemi, J. V., Timonen, H., Kangasluoma, J.,  
752 Tham, Y. J., Baalbaki, R., Sipilä, M., Salo, L., Lintusaari, H., Portin, H., Teinilä, K., Aurela, M., Dal Maso, M.,  
753 Rönkkö, T., Petäjä, T., and Paasonen, P.: Measurement report: The influence of traffic and new particle formation on  
754 the size distribution of 1-800nm particles in Helsinki-a street canyon and an urban background station comparison,  
755 *Atmos. Chem. Phys.*, 21, 9931–9953, <https://doi.org/10.5194/ACP-21-9931-2021>, 2021.
- 756 Olin, M., Kuuluvainen, H., Aurela, M., Kalliokoski, J., Kuittinen, N., Isotalo, M., Timonen, H. J., Niemi, J. V., Rönkkö,  
757 T., and Dal Maso, M.: Traffic-originated nanocluster emission exceeds H<sub>2</sub>SO<sub>4</sub>-driven photochemical new particle  
758 formation in an urban area, *Atmos. Chem. Phys.*, 20, 1–13, <https://doi.org/10.5194/acp-20-1-2020>, 2020.
- 759 Paatero, P.: Least squares formulation of robust non-negative factor analysis, *Chemom. Intell. Lab. Syst.*, 37, 23–35,  
760 [https://doi.org/10.1016/S0169-7439\(96\)00044-5](https://doi.org/10.1016/S0169-7439(96)00044-5), 1997.
- 761 Paatero, P.: The Multilinear Engine—A Table-Driven, Least Squares Program for Solving Multilinear Problems,  
762 Including the n-Way Parallel Factor Analysis Model, 8, 854–888, <https://doi.org/10.1080/10618600.1999.10474853>,  
763 1999.
- 764 Paatero, P. and Hopke, P. K.: Discarding or downweighting high-noise variables in factor analytic models, *Anal. Chim.*  
765 *Acta*, 490, 277–289, [https://doi.org/10.1016/S0003-2670\(02\)01643-4](https://doi.org/10.1016/S0003-2670(02)01643-4), 2003.
- 766 Paatero, P. and Tapper, U.: Positive matrix factorization: A non-negative factor model with optimal utilization of error  
767 estimates of data values, *Environmetrics*, 5, 111–126, <https://doi.org/10.1002/ENV.3170050203>, 1994.
- 768 Pandis, S. N., Harley, R. A., Cass, G. R., and Seinfeld, J. H.: Secondary organic aerosol formation and transport,  
769 *Atmos. Environ. Part A, Gen. Top.*, 26, 2269–2282, [https://doi.org/10.1016/0960-1686\(92\)90358-R](https://doi.org/10.1016/0960-1686(92)90358-R), 1992.
- 770 Peräkylä, O., Riva, M., Heikkinen, L., Quéléver, L., Roldin, P., and Ehn, M.: Experimental investigation into the  
771 volatilities of highly oxygenated organic molecules (HOMs), *Atmos. Chem. Phys.*, 20, 649–669,  
772 <https://doi.org/10.5194/acp-20-649-2020>, 2020.
- 773 Pope, C. A. and Dockery, D. W.: Health Effects of Fine Particulate Air Pollution: Lines that Connect, 56, 709–742,  
774 <https://doi.org/10.1080/10473289.2006.10464485>, 2012.
- 775 Pullinen, I., Schmitt, S., Kang, S., Sarrafzadeh, M., Schlag, P., Andres, S., Kleist, E., Mentel, T. F., Rohrer, F.,  
776 Springer, M., Tillmann, R., Wildt, J., Wu, C., Zhao, D., Wahner, A., and Kiendler-Scharr, A.: Impact of NO<sub>x</sub> on  
777 secondary organic aerosol (SOA) formation from  $\alpha$ -pinene and  $\beta$ -pinene photooxidation: The role of highly oxygenated  
778 organic nitrates, *Atmos. Chem. Phys.*, 20, 10125–10147, <https://doi.org/10.5194/ACP-20-10125-2020>, 2020.



- 779 Quelever, L. L. J., Kristensen, K., Normann Jensen, L., Rosati, B., Teiwes, R., Daellenbach, K. R., Peräkylä, O., Roldin,  
780 P., Bossi, R., Pedersen, H. B., Glasius, M., Bilde, M., and Ehn, M.: Effect of temperature on the formation of highly  
781 oxygenated organic molecules (HOMs) from alpha-pinene ozonolysis, *Atmos. Chem. Phys.*, 19, 7609–7625,  
782 <https://doi.org/10.5194/ACP-19-7609-2019>, 2019.
- 783 Rantala, P., Järvi, L., Taipale, R., Laurila, T. K., Patokoski, J., Kajos, M. K., Kurppa, M., Haapanala, S., Siivola, E.,  
784 Petäjä, T., Ruuskanen, T. M., and Rinne, J.: Anthropogenic and biogenic influence on VOC fluxes at an urban  
785 background site in Helsinki, Finland, *Atmos. Chem. Phys.*, 16, 7981–8007, <https://doi.org/10.5194/acp-16-7981-2016>,  
786 2016.
- 787 Richters, S., Herrmann, H., and Berndt, T.: Highly Oxidized RO<sub>2</sub> Radicals and Consecutive Products from the  
788 Ozonolysis of Three Sesquiterpenes, *Environ. Sci. Technol.*, 50, 2354–2362,  
789 [https://doi.org/10.1021/ACS.EST.5B05321/SUPPL\\_FILE/ES5B05321\\_SI\\_001.PDF](https://doi.org/10.1021/ACS.EST.5B05321/SUPPL_FILE/ES5B05321_SI_001.PDF), 2016.
- 790 Saarikoski, S., Hellén, H., Praplan, A. P., Schallhart, S., Clusius, P., Niemi, J. V., Kousa, A., Tykkä, T., Kouznetsov, R.,  
791 Aurela, M., Salo, L., Rönkkö, T., Barreira, L. M. F., Pirjola, L., and Timonen, H.: Characterization of volatile organic  
792 compounds and submicron organic aerosol in a traffic environment, *Atmos. Chem. Phys.*, 23, 2963–2982,  
793 <https://doi.org/10.5194/ACP-23-2963-2023>, 2023.
- 794 Seinfeld, J. H. and Pandis, S. N.: *Atmospheric Chemistry and Physics: From Air Pollution to Climate Change*, 2016.
- 795 Shen, H., Zhao, D., Pullinen, I., Kang, S., Vereecken, L., Fuchs, H., Acir, I. H., Tillmann, R., Rohrer, F., Wildt, J.,  
796 Kiendler-Scharr, A., Wahner, A., and Mentel, T. F.: Highly Oxygenated Organic Nitrates Formed from NO<sub>3</sub>Radical-  
797 Initiated Oxidation of  $\beta$ -Pinene, *Environ. Sci. Technol.*, 55, 15658–15671,  
798 [https://doi.org/10.1021/ACS.EST.1C03978/SUPPL\\_FILE/ES1C03978\\_SI\\_001.PDF](https://doi.org/10.1021/ACS.EST.1C03978/SUPPL_FILE/ES1C03978_SI_001.PDF), 2021.
- 799 Timonen, H., Karjalainen, P., Saukko, E., Saarikoski, S., Aakko-Saksa, P., Simonen, P., Murtonen, T., Dal Maso, M.,  
800 Kuuluvainen, H., Bloss, M., Ahlberg, E., Svenningsson, B., Pagels, J., Brune, W. H., Keskinen, J., Worsnop, D. R.,  
801 Hillamo, R., and Rönkkö, T.: Influence of fuel ethanol content on primary emissions and secondary aerosol formation  
802 potential for a modern flex-fuel gasoline vehicle, *Atmos. Chem. Phys.*, 17, 5311–5329, <https://doi.org/10.5194/ACP-17-5311-2017>, 2017.
- 804 Valiev, R. R., Hasan, G., Salo, V. T., Kubečka, J., and Kurten, T.: Intersystem Crossings Drive Atmospheric Gas-Phase  
805 Dimer Formation, *J. Phys. Chem. A*, 123, 6596–6604,  
806 [https://doi.org/10.1021/ACS.JPCA.9B02559/ASSET/IMAGES/LARGE/JP-2019-02559G\\_0006.JPEG](https://doi.org/10.1021/ACS.JPCA.9B02559/ASSET/IMAGES/LARGE/JP-2019-02559G_0006.JPEG), 2019.
- 807 Wang, Z., Ehn, M., Rissanen, M. P., Garmash, O., Quéléver, L., Xing, L., Monge-Palacios, M., Rantala, P., Donahue,  
808 N. M., Berndt, T., and Sarathy, S. M.: Efficient alkane oxidation under combustion engine and atmospheric conditions,  
809 *Commun. Chem.* 2021 41, 4, 1–8, <https://doi.org/10.1038/s42004-020-00445-3>, 2021.
- 810 Watson, J. G., Chow, J. C., and Fujita, E. M.: Review of volatile organic compound source apportionment by chemical  
811 mass balance, *Atmos. Environ.*, 35, 1567–1584, [https://doi.org/10.1016/S1352-2310\(00\)00461-1](https://doi.org/10.1016/S1352-2310(00)00461-1), 2001.
- 812 Wayne, R. P.: *Chemistry of atmospheres : an introduction to the chemistry of the atmospheres of earth, the planets, and  
813 their satellites*, 3rd ed., Oxford : Oxford University Press, 2000.



- 814 Wayne, R. P., Barnes, I., Biggs, P., Burrows, J. P., Canosa-Mas, C. E., Hjorth, J., Le Bras, G., Moortgat, G. K., Perner,  
815 D., Poulet, G., Restelli, G., and Sidebottom, H.: The nitrate radical: Physics, chemistry, and the atmosphere, *Atmos.*  
816 *Environ. Part A, Gen. Top.*, 25, 1–203, [https://doi.org/10.1016/0960-1686\(91\)90192-A](https://doi.org/10.1016/0960-1686(91)90192-A), 1991.
- 817 WHO: WHO global air quality guidelines: particulate matter (PM<sub>2.5</sub> and PM<sub>10</sub>), ozone, nitrogen dioxide, sulfur  
818 dioxide and carbon monoxide, 2021.
- 819 Yan, C., Nie, W., Aijälä, M., Rissanen, M. P., Canagaratna, M. R., Massoli, P., Junninen, H., Jokinen, T., Sarnela, N.,  
820 Häme, S. A. K., Schobesberger, S., Canonaco, F., Yao, L., Prévôt, A. S. H., Petäjä, T., Kulmala, M., Sipilä, M.,  
821 Worsnop, D. R., and Ehn, M.: Source characterization of highly oxidized multifunctional compounds in a boreal forest  
822 environment using positive matrix factorization, *Atmos. Chem. Phys.*, 16, 12715–12731, [https://doi.org/10.5194/acp-](https://doi.org/10.5194/acp-16-12715-2016)  
823 16-12715-2016, 2016.
- 824 Yan, C., Nie, W., Vogel, A. L., Dada, L., Lehtipalo, K., Stolzenburg, D., Wagner, R., Rissanen, M. P., Xiao, M.,  
825 Ahonen, L., Fischer, L., Rose, C., Bianchi, F., Gordon, H., Simon, M., Heinritzi, M., Garmash, O., Roldin, P., Dias, A.,  
826 Ye, P., Hofbauer, V., Amorim, A., Bauer, P. S., Bergen, A., Bernhammer, A. K., Breitenlechner, M., Brilke, S.,  
827 Buchholz, A., Mazon, S. B., Canagaratna, M. R., Chen, X., Ding, A., Dommen, J., Draper, D. C., Duplissy, J., Frege,  
828 C., Heyn, C., Guida, R., Hakala, J., Heikkinen, L., Hoyle, C. R., Jokinen, T., Kangasluoma, J., Kirkby, J., Kontkanen,  
829 J., Kürten, A., Lawler, M. J., Mai, H., Mathot, S., Mauldin, R. L., Molteni, U., Nichman, L., Nieminen, T., Nowak, J.,  
830 Ojdanic, A., Onnela, A., Pajunoja, A., Petäjä, T., Piel, F., Quéléver, L. L. J., Sarnela, N., Schallhart, S., Sengupta, K.,  
831 Sipilä, M., Tomé, A., Tröstl, J., Väisänen, O., Wagner, A. C., Ylisirniö, A., Zha, Q., Baltensperger, U., Carslaw, K. S.,  
832 Curtius, J., Flagan, R. C., Hansel, A., Riipinen, I., Smith, J. N., Virtanen, A., Winkler, P. M., Donahue, N. M.,  
833 Kerminen, V. M., Kulmala, M., Ehn, M., Worsnop, D. R., Voge, A. L., Dada, L., Lehtipalo, K., Stolzenburg, D., Wagner,  
834 R., Rissanen, M. P., Xiao, M., Ahonen, L., Fischer, L., Rose, C., Bianchi, F., Gordon, H., Simon, M., Heinritzi, M.,  
835 Garmash, O., et al.: Size-dependent influence of nox on the growth rates of organic aerosol particles, *Sci. Adv.*, 6,  
836 4945–4972, [https://doi.org/10.1126/SCIADV.AAY4945/SUPPL\\_FILE/AAY4945\\_SM.PDF](https://doi.org/10.1126/SCIADV.AAY4945/SUPPL_FILE/AAY4945_SM.PDF), 2020.
- 837 Yan, C., Shen, Y., Stolzenburg, D., Dada, L., Qi, X., Hakala, S., Sundström, A.-M., Guo, Y., Lipponen, A., Kokkonen,  
838 T. V., Kontkanen, J., Cai, R., Cai, J., Chan, T., Chen, L., Chu, B., Deng, C., Du, W., Fan, X., He, X.-C., Kangasluoma,  
839 J., Kujansuu, J., Kurppa, M., Li, C., Li, Y., Lin, Z., Liu, Y., Liu, Y., Lu, Y., Nie, W., Pulliainen, J., Qiao, X., Wang, Y.,  
840 Wen, Y., Wu, Y., Yang, G., Yao, L., Yin, R., Zhang, G., Zhang, S., Zheng, F., Zhou, Y., Arola, A., Tamminen, J.,  
841 Paasonen, P., Sun, Y., Wang, L., Donahue, N. M., Liu, Y., Bianchi, F., Daellenbach, K. R., Worsnop, D. R., Kerminen,  
842 V.-M., Petäjä, T., Ding, A., Jiang, J., and Kulmala, M.: The effect of COVID-19 restrictions on atmospheric new  
843 particle formation in Beijing, *Atmos. Chem. Phys.*, 22, 12207–12220, <https://doi.org/10.5194/ACP-22-12207-2022>,  
844 2022.
- 845 Zha, Q., Yan, C., Junninen, H., Riva, M., Sarnela, N., Aalto, J., Quéléver, L., Schallhart, S., Dada, L., Heikkinen, L.,  
846 Peräkylä, O., Zou, J., Rose, C., Wang, Y., Mammarella, I., Katul, G., Vesala, T., Worsnop, D. R., Kulmala, M., Petäjä,  
847 T., Bianchi, F., and Ehn, M.: Vertical characterization of highly oxygenated molecules (HOMs) below and above a  
848 boreal forest canopy, *Atmos. Chem. Phys.*, 18, 17437–17450, <https://doi.org/10.5194/ACP-18-17437-2018>, 2018.
- 849 Zhang, Q., Jimenez, J. L., Canagaratna, M. R., Ulbrich, I. M., Ng, N. L., Worsnop, D. R., and Sun, Y.: Understanding  
850 atmospheric organic aerosols via factor analysis of aerosol mass spectrometry: A review, *Anal. Bioanal. Chem.*, 401,  
851 3045–3067, <https://doi.org/10.1007/S00216-011-5355-Y/FIGURES/10>, 2011.





- 852 Zhang, Y., Peräkylä, O., Yan, C., Heikkinen, L., Äijälä, M., Daellenbach, K. R., Zha, Q., Riva, M., Garmash, O.,  
853 Junninen, H., Paatero, P., Worsnop, D., and Ehn, M.: A novel approach for simple statistical analysis of high-resolution  
854 mass spectra, *Atmos. Meas. Tech.*, 12, 3761–3776, <https://doi.org/10.5194/amt-12-3761-2019>, 2019.
- 855 Zhang, Y., Peräkylä, O., Yan, C., Heikkinen, L., Äijälä, M., Daellenbach, K. R., Zha, Q., Riva, M., Garmash, O.,  
856 Junninen, H., Paatero, P., Worsnop, D., and Ehn, M.: Insights into atmospheric oxidation processes by performing  
857 factor analyses on subranges of mass spectra, *Atmos. Chem. Phys.*, 20, 5945–5961, [https://doi.org/10.5194/acp-20-](https://doi.org/10.5194/acp-20-5945-2020)  
858 5945-2020, 2020.
- 859 Zhang, Y., Li, D., Ma, Y., Dubois, C., Wang, X., Perrier, S., Chen, H., Wang, H., Jing, S., Lu, Y., Lou, S., Yan, C., Nie,  
860 W., Chen, J., Huang, C., George, C., and Riva, M.: Field Detection of Highly Oxygenated Organic Molecules in  
861 Shanghai by Chemical Ionization-Orbitrap, *Environ. Sci. Technol.*, 56, 7608–7617,  
862 <https://doi.org/10.1021/ACS.EST.1C08346>/ASSET/IMAGES/LARGE/ES1C08346\_0005.JPEG, 2022.
- 863